

# Critical behavior of the (2+1)-dimensional Thirring model

Lukas Janssen\* and Holger Gies†

*Theoretisch-Physikalisches Institut, Friedrich-Schiller-Universität Jena, Max-Wien-Platz 1, 07743 Jena, Germany*

(Dated: August 16, 2012)

We investigate chiral symmetry breaking in the (2+1)-dimensional Thirring model as a function of the coupling as well as the Dirac flavor number  $N_f$  with the aid of the functional renormalization group. For small enough flavor number  $N_f < N_f^{\text{cr}}$ , the model exhibits a chiral quantum phase transition for sufficiently large coupling. We compute the critical exponents of this second order transition as well as the fermionic and bosonic mass spectrum inside the broken phase within a next-to-leading order derivative expansion. We also determine the quantum critical behavior of the many-flavor transition which arises due to a competition between vector and chiral-scalar channel and which is of second order as well. Due to the problem of competing channels, our results rely crucially on the RG technique of dynamical bosonization. For the critical flavor number, we find  $N_f^{\text{cr}} \simeq 5.1$  with an estimated systematic error of approximately one flavor.

## I. INTRODUCTION AND SUMMARY

**Introduction.** Since the advent of graphene [1] there has been an enormous amount of renewed interest in (2+1)-dimensional relativistic fermion systems. Various variants of (2+1)d quantum electrodynamics [2–18] and the (2+1)d Thirring model [19–33] are actively discussed as effective descriptions of graphene’s exceptional electronic properties [34–41]. Moreover, they are likewise intrinsically interesting: in these models the number of fermion flavors  $N_f$  serves as a control parameter for a quantum phase transition at a critical value  $N_f^{\text{cr}}$ . Several previous works provide a substantial amount of evidence that chiral symmetry breaking ( $\chi$ SB) may be prohibited even for arbitrarily large coupling if  $N_f > N_f^{\text{cr}}$  [22, 24–31]. This is a similarity to many-flavor non-abelian gauge theories in four dimensions which are used for particle physics models for dynamical electroweak symmetry breaking [42–44]. However, the search for the quantum critical point has so far been rather challenging: in the Thirring model different approximate solutions to the Dyson-Schwinger equations (DSE) yielded values between  $N_f^{\text{cr}} \simeq 3.24$  [22] and  $N_f^{\text{cr}} = \infty$  [23]. By constructing an effective potential for the chiral order parameter, up to leading order of the  $1/N_f$  expansion  $N_f^{\text{cr}} = 2$  has been found [26]. Extensive Monte Carlo simulations point to  $N_f^{\text{cr}} \simeq 6.6$  [31]. The true value of  $N_f^{\text{cr}}$  is of decisive relevance for the applicability of such relativistic fermion effective theories for condensed matter systems, where the number of flavors is typically  $N_f = 2$ . If  $N_f = 2$  is near  $N_f^{\text{cr}}$ , the properties of the quantum critical regime could take an important influence on physical effects corresponding to dynamical mass generation in the effective (strongly-coupled) theories. Understanding such a semimetal-Mott insulator transition is also desirable from a technological point of view, e.g., with the ultimate aim of engineering the band gap in graphene-like systems.

In addition to the significant quantitative discrepancies observed in the literature, a more detailed comparison of the critical behavior close to  $N_f^{\text{cr}}$  reported in those studies reveals our insufficient understanding of fermionic field theories in the nonperturbative domain: Kondo [26] reports a *second-order* phase transition with the usual power-law behavior as a function of the control parameter  $N_f$ . By contrast, in the DSE studies [24, 25] an essential scaling behavior of the Kosterlitz-Thouless type has been found, that is to say, a phase transition of *infinite* order. As argued in [31], the nature of the transition in these studies appears to depend on whether the strong-coupling limit is taken before or after  $N_f \nearrow N_f^{\text{cr}}$ . The scaling analysis on the lattice [31, 32] is consistent with a power-law behavior corresponding to a second-order phase transition which qualitatively confirms, but quantitatively deviates from the Kondo scenario [26].

In the present work, we confront the functional renormalization group (RG) approach with the puzzles given by the (2+1)d chiral fermion systems at criticality. The question is: What is the nature of the  $\chi$ SB phase transition being controlled by either the bare coupling  $g$  (for fixed  $N_f < N_f^{\text{cr}}$ ) or the number of flavors  $N_f$  (for fixed  $g > g_{\text{cr}}$ )? What are, if applicable, the corresponding exponents determining the critical behavior? Naively, a universal answer may not be apparent as (2+1)d fermion models are perturbatively nonrenormalizable. However, rather than inherent inconsistencies, this difficulty may reflect the failure of the perturbative approach [45–48]. In fact, there is a large body of evidence for nonperturbative renormalizability to all orders in a large- $N_f$  expansion [19–23] and, more recently, also beyond the  $1/N_f$  expansion from a functional RG approach [49, 50]. As a bottom line, (2+1)-dimensional fermion models appear to be a paradigm example for asymptotically safe theories [51–55] that are UV complete due to the existence of interacting UV fixed points.

In the remainder of this section, we briefly summarize our findings, starting with a short review of a preceding fermionic RG analysis [49]. All technical details and a proper embedding and comparison to the literature is

\* lukas.janssen@uni-jena.de

† holger.gies@uni-jena.de

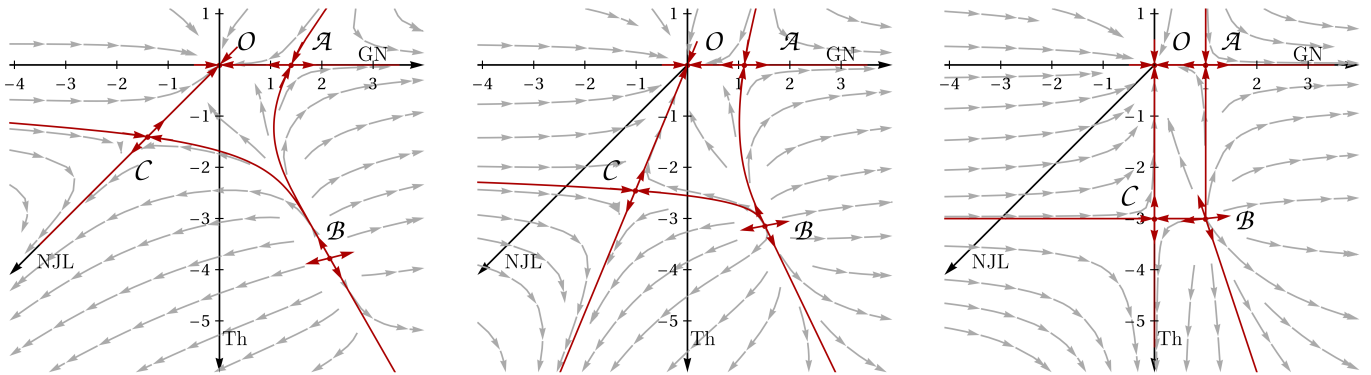


FIG. 1. Fermionic RG flow in the Gross-Neveu (GN) – Thirring (Th) coupling plane, compiled from Refs. [49, 50]. The angle bisector in the 3rd quadrant defines the theories with pure Nambu-Jona-Lasinio (NJL) interactions. Left panel: for  $N_f = 1.75$  the Thirring fixed point  $\mathcal{C}$  lies exactly on the NJL axis with  $\mathcal{L}_{\text{int}} \propto (S)^2$ . Right panel: in the limit  $N_f \rightarrow \infty$ , the Thirring fixed point  $\mathcal{C}$  lies on the Thirring axis with  $\mathcal{L}_{\text{int}} \propto (V)^2$ . Middle panel: for intermediate flavor number (here  $N_f \simeq 5$ ), we expect a competition between the scalar-type NJL channel  $(S)^2$  and the vector-type Thirring channel  $(V)^2$ .

deferred to the following sections.

**Competing channels in the (2+1)d Thirring model.** Conventionally, the Thirring model in 2+1 dimensions is defined by the Lagrangian

$$\mathcal{L} = \mathcal{L}_{\text{kin}} + \mathcal{L}_{\text{int}} = \bar{\psi}^a i \not{\partial} \psi^a + \frac{\bar{g}}{2N_f} (\bar{\psi}^a \gamma_\mu \psi^a)^2, \quad (1)$$

with  $N_f$  flavors of massless four-component Dirac spinors  $\psi^a$ , i.e.,  $a = 1, \dots, N_f$ . The microscopic theory has a chiral symmetry  $U(2N_f)$ , cf. Sec. II. Depending on the value of the four-fermi coupling  $\bar{g}$  and the number of flavors  $N_f$ , a fermion mass can be dynamically generated, which breaks the chiral symmetry spontaneously. Upon integrating out fluctuations, further interaction terms, being compatible with the present  $U(2N_f)$  symmetry, are generated by the RG transformations. On the four-fermi level there are three further interactions besides the Thirring term  $\sim (\bar{\psi} \gamma_\mu \psi)^2$ : a flavor-singlet pseudo-scalar channel (Gross-Neveu interaction), a flavor-nonsinglet scalar channel (Nambu-Jona-Lasinio interaction), and a flavor-nonsinglet axial channel. However, not all of these terms are independent in the pointlike limit: due to the Fierz identities we can always choose an arbitrary subset of two terms and write the respective other two as a linear combination of these. A full basis is therefore given, e.g., by the Thirring and the Gross-Neveu interaction. The RG flow of the dimensionless couplings in this basis is depicted in Fig. 1. The vertical (horizontal) axis defines the theories with pure Thirring (Gross-Neveu) interaction. We refer to this axis as “Thirring axis” (“Gross-Neveu axis”). The angle bisector in the third quadrant defines the theories with pure Nambu-Jona-Lasinio (NJL) interaction, which we refer to as “NJL axis”. In a functional RG analysis (the technique is sketched in Sec. III), we find two interacting fixed points  $\mathcal{A}$ ,  $\mathcal{B}$ , and  $\mathcal{C}$  besides the Gaussian fixed point  $\mathcal{O}$ . For the theories defined by the microscopic Lagrangian (1) being purely on the Thirring axis, we find two different phases, which are separated

by the separatrix through the fixed points  $\mathcal{B}$  and  $\mathcal{C}$  (red curve in Fig. 1): If we start the RG flow in the UV with a microscopic coupling on the Thirring axis above the separatrix, the couplings eventually flow to the noninteracting Gaussian fixed point  $\mathcal{O}$ ; if we start below this curve, the four-fermi couplings grow large in the IR. In the vicinity of the critical coupling, the behavior of the system is governed by the interacting fixed point  $\mathcal{C}$ , as all trajectories are initially attracted toward this fixed point. We refer to this fixed point as “Thirring fixed point”. We associate all trajectories emanating from  $\mathcal{C}$  with UV complete fully renormalized versions of the (2+1)d Thirring model. However, we emphasize that the Thirring fixed point only in the strict large- $N_f$  limit lies directly on the Thirring axis: even if absent on the microscopic scale, a second coupling besides the Thirring coupling will always be generated by the fluctuations for finite  $N_f$ .

We now give a heuristic argument for the occurrence of the critical flavor number [49, 50]. Let us first consider the (unphysical) flavor number  $N_f = 1.75$ , where the Thirring fixed point  $\mathcal{C}$  lies exactly on the NJL axis (left panel of Fig. 1). In this specific case, the NJL axis is an IR attractive hyperplane and the RG flow of the Thirring model for sufficiently large (negative) coupling is dominated by a divergent NJL coupling. A divergent scalar-type four-fermi coupling at finite RG scale signals bound-state formation in that channel and can be associated with the dynamical generation of the corresponding order parameter, in this case the chiral order parameter  $\langle \bar{\psi} \psi \rangle$ . We therefore predict that spontaneous breaking of chiral symmetry occurs due to a dominance of the scalar-type NJL channel. Since the fixed-point positions change only smoothly with  $N_f$ , we expect this conclusion to hold also for small deviations from  $N_f = 1.75$ . By contrast, for very large flavor number, the IR attractive hyperplane with the Thirring fixed point  $\mathcal{C}$  is located on the Thirring axis, i.e., at vanishing NJL coupling (right panel of Fig. 1). In other words, the RG flow

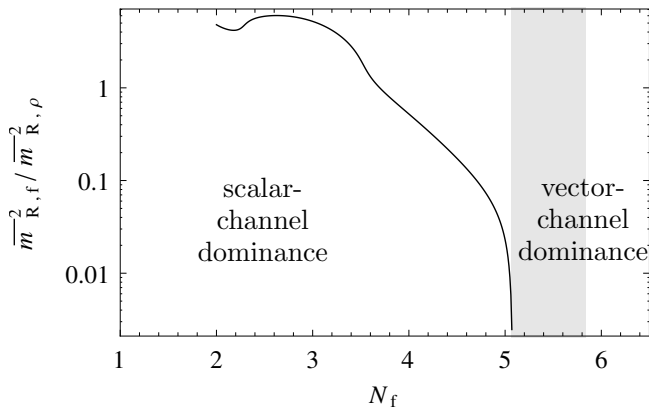


FIG. 2. Log-plot of the dynamically generated renormalized fermion mass  $\bar{m}_{R,f}^2$  in units of the renormalized mass  $\bar{m}_{R,\rho}^2$  of a radial bosonic excitation on top of the chiral condensate. Our estimates for the critical flavor number,  $N_f^{\text{cr}} \simeq 5.1$  for a linear regulator is amended by an error bar (gray shaded area) obtained by varying the regularization scheme (e.g.,  $N_f^{\text{cr}} \simeq 5.8$  for the sharp cutoff).

is governed by a strong vector-channel dominance, which generically inhibits  $\chi\text{SB}$ . For intermediate flavor number (middle panel of Fig. 1), we thus expect a transition between the scalar-type NJL channel, which triggers  $\chi\text{SB}$ , and the vector-type Thirring channel, inhibiting  $\chi\text{SB}$ .

**Dynamical boson fields.** A more quantitative picture of this quantum phase transition is difficult to obtain in the purely fermionic language with point-like interactions. A quantitative RG analysis requires the inclusion of dynamical chiral and vector bosonic degrees of freedom, see Secs. IV-VI, in order to study the interplay of these competing channels as a function of  $N_f$ . This is the objective of this paper. In particular, we will show how the competition between the NJL (dominant for small  $N_f$ ) and the Thirring channel (dominant for large  $N_f$ ) leads to a decrease of the dynamically generated fermion mass with  $N_f$ , culminating in a complete vanishing at  $N_f^{\text{cr}} \simeq 5.1$  (linear regulator); cf. Fig. 2. We can also map out the order of the phase transition as a function of  $N_f$ : in Fig. 3 we depict the order parameter  $\langle\varphi\rangle \propto \langle\bar{\psi}\psi\rangle$  vs.  $N_f^{\text{cr}}/N_f - 1$  in a double-log plot, showing very good compatibility with a second order phase transition with scaling behavior  $\langle\varphi\rangle \propto (N_f^{\text{cr}}/N_f - 1)^b$  and the universal critical exponent  $b \simeq 0.44$ . To avoid any possibility of confusion, let us denote the critical exponents for the phase transition as a function of  $N_f$  (at fixed overcritical coupling) with Latin letters, and the ones for the phase transition as a function of the coupling (at fixed  $N_f < N_f^{\text{cr}}$ ) with Greek letters. We find that the latter phase transition is also of second order, the critical behavior of which is determined by the RG flow in the vicinity of the Thirring fixed point. We give our predictions for the universal critical exponents  $\nu$ ,  $\omega$ , and  $\eta_\phi^*$  for various flavor numbers in Table II on page 15.

In addition to our quantitative results, it is one of

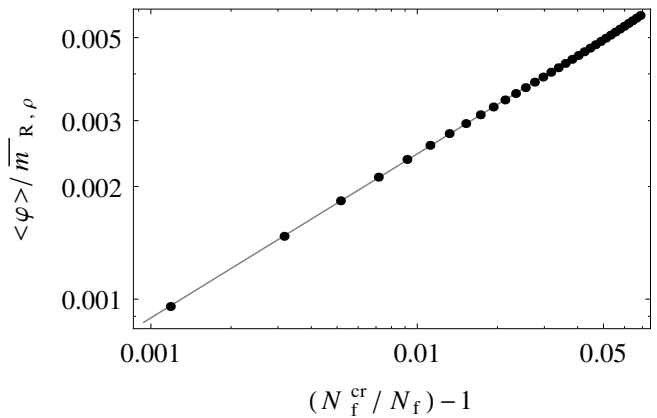


FIG. 3. Order parameter (black dots) vs.  $N_f^{\text{cr}}/N_f - 1$  in a double-log plot, showing very good compatibility with power-law scaling behavior  $\langle\varphi\rangle \propto (N_f^{\text{cr}}/N_f - 1)^b$ . The slope of the regression line (gray) is  $b \simeq 0.44$ .

our most important observations that a simple partial bosonization à la Hubbard-Stratonovich is not sufficient for resolving the competition between the various channels. A method to deal with this challenging problem is *dynamical bosonization*, as detailed in Sec. VII. As there is already a large variety of analytical as well as numerical studies on the (2+1)d Thirring model in the literature – with partly contradictory results – we finally perform a careful and critical comparison between the literature and our work in Sec. X.

## II. CONDENSATION CHANNELS AND FIERZ BASIS

Let us start by presenting our conventions for general fermionic models in  $d = 2 + 1$  Euclidean dimensions with local quartic self-interaction, being invariant under the full symmetry of the noninteracting theory. We concentrate on representations of the Dirac algebra as they occur naturally in the language of effective theories describing electronic interactions on graphene's honeycomb lattice [34–40] and in cuprates [56–61].

The models shall satisfy Osterwalder-Schrader positivity [62], requiring invariance of the action under generalized complex conjugation defined by  $\psi^\dagger := i\bar{\psi}\gamma_3$  and a simultaneous reflection of the Euclidean time coordinate, which we choose to be  $x_3$ . For a detailed discussion of our chiral conventions, see Refs. [63, 64]. Consider the  $4 \times 4$  *reducible* representation

$$\gamma_\mu = \begin{pmatrix} 0 & -i\sigma_\mu \\ i\sigma_\mu & 0 \end{pmatrix}, \quad \mu = 1, 2, 3, \quad (2)$$

of the Dirac algebra  $\{\gamma_\mu, \gamma_\nu\} = 2\delta_{\mu\nu}$ , reminiscent of the chiral representation in four dimensions. Here,  $\{\sigma_\mu\}_{\mu=1,2,3}$  denote the standard  $2 \times 2$  Pauli matrices. In this formulation, the Dirac fermions thus have four components. There are now *two* other  $4 \times 4$  matrices, which

anticommute with all  $\gamma_\mu$  as well as with each other,

$$\gamma_4 = \begin{pmatrix} 0 & \mathbb{1}_2 \\ \mathbb{1}_2 & 0 \end{pmatrix} \quad \text{and} \quad \gamma_5 = \gamma_1\gamma_2\gamma_3\gamma_4 = \begin{pmatrix} \mathbb{1}_2 & 0 \\ 0 & -\mathbb{1}_2 \end{pmatrix}. \quad (3)$$

Together with

$$\mathbb{1}_4, \gamma_{\mu\nu} := \frac{i}{2}[\gamma_\mu, \gamma_\nu] \ (\mu < \nu), \ i\gamma_\mu\gamma_4, \ i\gamma_\mu\gamma_5, \ \gamma_{45} := i\gamma_4\gamma_5, \quad (4)$$

these 16 matrices form a complete basis of the  $4 \times 4$  Dirac algebra,

$$\{\gamma_A\}_{A=1,\dots,16} = \{\mathbb{1}_4, \gamma_\mu, \gamma_4, \gamma_{\mu\nu}, i\gamma_\mu\gamma_4, i\gamma_\mu\gamma_5, \gamma_{45}, \gamma_5\}. \quad (5)$$

The general fermionic Lagrangian compatible with  $U(2N_f)$  chiral as well as  $\mathcal{C}$ ,  $\mathcal{P}$ , and  $\mathcal{T}$  discrete symmetry has the form [10, 11, 36, 49, 50]

$$\begin{aligned} \mathcal{L} = & \bar{\psi}^a i\not{\partial}\psi^a + \frac{\bar{g}_1}{2N_f}(V)^2 + \frac{\bar{g}_2}{2N_f}(S)^2 + \frac{\bar{g}_3}{2N_f}(P)^2 \\ & + \frac{\bar{g}_4}{2N_f}(A)^2, \end{aligned} \quad (6)$$

with the bare couplings  $\bar{g}_{1,\dots,4}$  carrying an inverse mass dimension, and with the flavor singlet channels

$$(V)^2 := (\bar{\psi}^a \gamma_\mu \psi^a)^2, \quad (P)^2 := (\bar{\psi}^a \gamma_{45} \psi^a)^2, \quad (7)$$

and the flavor nonsinglet channels

$$\begin{aligned} (S)^2 := & (\bar{\psi}^a \psi^b)^2 - (\bar{\psi}^a \gamma_4 \psi^b)^2 - (\bar{\psi}^a \gamma_5 \psi^b)^2 \\ & + (\bar{\psi}^a \gamma_{45} \psi^b)^2, \end{aligned} \quad (8)$$

$$\begin{aligned} (A)^2 := & (\bar{\psi}^a \gamma_\mu \psi^b)^2 + \frac{1}{2}(\bar{\psi}^a \gamma_{\mu\nu} \psi^b)^2 - (\bar{\psi}^a i\gamma_\mu \gamma_4 \psi^b)^2 \\ & - (\bar{\psi}^a i\gamma_\mu \gamma_5 \psi^b)^2. \end{aligned} \quad (9)$$

Here, we have abbreviated  $(\psi^a \psi^b)^2 \equiv \psi^a \psi^b \psi^b \psi^a$ , etc.  $N_f$  denotes the number of four-component (reducible) Dirac spinors, such that  $a, b = 1, \dots, N_f$ . By means of the Fierz identities,

$$(V)^2 + (S)^2 + (P)^2 = 0, \quad -4(V)^2 - 3(S)^2 + (A)^2 = 0, \quad (10)$$

any two four-fermi terms can be rewritten as a linear combination of the remaining two. Put differently, by adding a linear combination of Eqs. (10) with coefficients  $\alpha_i \in \mathbb{R}$  (in units of some inverse mass scale) to the Lagrangian (6),

$$\begin{aligned} \mathcal{L} = & \bar{\psi}^a i\not{\partial}\psi^a + \frac{1}{2N_f}(\bar{g}_1 + \alpha_1 - 4\alpha_2)(V)^2 \\ & + \frac{1}{2N_f}(\bar{g}_2 + \alpha_1 - 3\alpha_2)(S)^2 + \frac{1}{2N_f}(\bar{g}_3 + \alpha_1)(P)^2 \\ & + \frac{1}{2N_f}(\bar{g}_4 + \alpha_2)(A)^2, \end{aligned} \quad (11)$$

the  $\alpha_i$  are redundant parameters: in a full computation of the functional integral, any physical quantity has to be independent of  $\alpha_i$ . This no longer necessarily remains true once approximations are employed. A particular example is given by mean-field theory, where this so-called ‘‘Fierz ambiguity’’ or ‘‘mean-field ambiguity’’ can have a sizable influence on the results, limiting its quantitative reliability [65]. The ambiguity is absent in the purely fermionic renormalization group equations with momentum-independent couplings [49]. A solution of the Fierz ambiguity using the functional RG in a partially bosonized setting [66] requires dynamical bosonization [67] as will become important below. An alternative approach in the purely fermionic description employs a new parametrization of the momentum structure of the four-fermi couplings, see [68].

The particular choice of couplings  $\bar{g}$  and  $\tilde{\bar{g}}$  as used in [49] is recovered for  $\alpha_1 = -\bar{g}_2 - 3\bar{g}_4$  and  $\alpha_2 = -\bar{g}_4$  and the definition

$$\bar{g} := \bar{g}_1 - \bar{g}_2 + \bar{g}_4, \quad (12)$$

$$\tilde{\bar{g}} := -\bar{g}_2 + \bar{g}_3 - 3\bar{g}_4. \quad (13)$$

The Thirring (vertical) axis in Fig. 1 corresponds to  $\bar{g}$ , whereas the Gross-Neveu (horizontal) axis is associated with  $\tilde{\bar{g}}$  (more precisely with their dimensionless counterparts). Upon choosing  $\alpha_1 = -\bar{g}_3$  and  $\alpha_2 = -\bar{g}_4$ , the Lagrangian reads

$$\begin{aligned} \mathcal{L} = & \bar{\psi}^a i\not{\partial}\psi^a - \frac{\bar{g}_V}{2N_f} (\bar{\psi}^a \gamma_\mu \psi^a)^2 + \frac{\bar{g}_\phi}{4N_f} \left[ (\bar{\psi}^a \psi^b)^2 \right. \\ & \left. - (\bar{\psi}^a \gamma_4 \psi^b)^2 - (\bar{\psi}^a \gamma_5 \psi^b)^2 + (\bar{\psi}^a \gamma_{45} \psi^b)^2 \right], \end{aligned} \quad (14)$$

where we have defined the new couplings

$$\bar{g}_V := -\bar{g}_1 + \bar{g}_3 - 4\bar{g}_4 = \tilde{\bar{g}} - \bar{g}, \quad (15)$$

$$\bar{g}_\phi := 2(\bar{g}_2 - \bar{g}_3 + 3\bar{g}_4) = -2\tilde{\bar{g}}. \quad (16)$$

This form is convenient in order to investigate the competition between the vector  $(V)^2$  and NJL-type  $(S)^2$  channel for  $N_f \geq 2$ . For  $N_f = 1$  one might however choose yet another basis,

$$\begin{aligned} \mathcal{L}^{N_f=1} = & \bar{\psi} i\not{\partial}\psi + \frac{2\bar{g}_1 - \bar{g}_3 + 3\bar{g}_4}{4} (\bar{\psi} \gamma_\mu \psi)^2 \\ & + \frac{2\bar{g}_2 - \bar{g}_3 + 3\bar{g}_4}{4} \left[ (\bar{\psi} \psi)^2 - (\bar{\psi} \gamma_4 \psi)^2 - (\bar{\psi} \gamma_5 \psi)^2 \right]. \end{aligned} \quad (17)$$

The Dirac spinors can be projected onto their Weyl components, using the projectors<sup>1</sup>

$$P_{L/R}^{(45)} = \frac{1}{2}(1 \pm \gamma_{45}) = \frac{1}{2} \begin{pmatrix} \mathbb{1}_2 & (-i)\mathbb{1}_2 \\ i\mathbb{1}_2 & \mathbb{1}_2 \end{pmatrix}, \quad (18)$$

<sup>1</sup> We note that one could choose more adapted representations in which  $\gamma_{45} = \text{diag}(\mathbb{1}_2, -\mathbb{1}_2)$  and thus the Weyl spinor  $\chi^a$  ( $\chi^{a+N_f}$ ) is simply given by the upper (lower) two components of the Dirac spinor  $\psi^a$ . The ‘‘graphene representation’’ [35, 36] is of this type.

where the last equation holds for the representation (2)–(3). This suggests the decomposition [10]

$$\psi^a = \frac{1}{\sqrt{2}} \begin{pmatrix} \chi^a + \chi^{a+N_f} \\ i(\chi^a - \chi^{a+N_f}) \end{pmatrix}, \quad (19)$$

$$\bar{\psi}^a = \frac{1}{\sqrt{2}} (\bar{\chi}^a - \bar{\chi}^{a+N_f}, (-i)(\bar{\chi}^a + \bar{\chi}^{a+N_f})), \quad (20)$$

$a = 1, \dots, N_f$ , with the definition of the Dirac adjoint  $\bar{\chi}$  chosen such that  $\chi^\dagger := i\bar{\chi}\sigma_3$  in agreement with  $\psi^\dagger := i\bar{\psi}\gamma_3$ . In other words, we can trade the  $N_f$  flavors of four-component spinors  $\psi$  for  $2N_f$  flavors of two-component spinors  $\chi$ . Therewith, the theory (14) can equivalently be described using an irreducible representation by an action consisting of  $2N_f$  flavors of two-component Weyl spinors  $\bar{\chi}, \chi$ ,

$$\mathcal{L} = \bar{\chi}^i i\not{\partial}\chi^i - \frac{\bar{g}_V}{2N_f} (\bar{\chi}^i \sigma_\mu \chi^i)^2 + \frac{\bar{g}_\phi}{2N_f} (\bar{\chi}^i \chi^j)^2, \quad (21)$$

where we have introduced the collective indices  $i, j$ , running over  $2N_f$  flavors,  $i, j = 1, \dots, 2N_f$ . It is this representation in which the  $U(2N_f)$  symmetry is manifest,

$$U(2N_f): \quad \chi^i \mapsto U^{ij}\chi^j, \quad \bar{\chi}^i \mapsto \bar{\chi}^j (U^\dagger)^{ji}, \quad U \in U(2N_f). \quad (22)$$

Below, we use this formulation, allowing us to conveniently introduce collective low-energy degrees of freedom.

### III. FUNCTIONAL RG APPROACH

The functional RG has become a standard method to investigate strongly-interacting field theories. In particular for critical phenomena, it is a versatile tool yielding quantitatively accurate results in many cases. Conceptually, the functional RG can be formulated in terms of an RG flow equation for a generating functional. Among the various formulations, the Wetterich equation [69] representing the flow equation for the effective average action has become the most widely used method owing to its flexibility, numerical stability and direct applicability to physics problems. For reviews see [70–76] and [77–79] for a particular emphasis on fermionic systems. Prominent benchmark examples in three dimensions are bosonic  $O(N)$  models [70, 80, 81] or the Gross-Neveu model [55, 82, 83].

The effective average action  $\Gamma_k$  is a scale-dependent variant of the standard generating functional for 1PI correlation functions. The scale  $k$  denotes an IR regulator scale separating the UV modes with momenta  $p^2 > k^2$  which have already been integrated out from the IR modes with momenta  $p^2 < k^2$  which still have to be averaged over.  $\Gamma_k$  is constructed in such a way that it can be related to the microscopic bare action  $\Gamma_{k \rightarrow \Lambda} \rightarrow S_\Lambda$  if  $k$  approaches the UV cutoff scale  $\Lambda$ , while it approaches the standard full effective action in the IR limit  $\Gamma_{k \rightarrow 0} \rightarrow \Gamma$ .

The effective average action obeys the Wetterich equation [69],

$$\partial_t \Gamma_k[\Phi] = \frac{1}{2} \text{STr} \left( \frac{\partial_t R_k}{\Gamma_k^{(2)}[\Phi] + R_k} \right), \quad \partial_t \equiv k \frac{\partial}{\partial k}, \quad (23)$$

where the trace runs over all internal degrees of freedom (flavor, spinor, momentum) as well as field degrees of freedom. Here, the field  $\Phi$  represents a collective field variable including all bosonic or fermionic fields under consideration. The denominator contains the second functional derivative  $\Gamma_k^{(2)}[\Phi]$  with respect to the field  $\Phi$  together with the regulator function  $R_k$  which can be thought of as a momentum-dependent mass term.

Once the initial condition of the flow is fixed in terms of the microscopic action  $S_\Lambda$ , the exact solution of Eq. (23) provides us with an RG trajectory of  $\Gamma_k$  in the theory space of action functionals, the end-point at  $k = 0$  of which is the exact effective action  $\Gamma$ .

As it is, in practice, difficult to find exact solutions, the Wetterich equation can also be used to find approximate solutions by means of systematic and consistent expansion schemes of the effective action. While perturbation theory constitutes one such expansion scheme, nonperturbative schemes based on vertex or operator expansions are equally legitimate and clearly superior at intermediate or even strong coupling. For critical phenomena and the analysis of long-range order, derivative expansions in terms of the order-parameter fields have become a standard tool yielding accurate results in many nontrivial examples. In the present work, we will also use a truncation of the effective action in the spirit of the derivative expansion. However, as the chiral order parameter field is bosonic, the derivative expansion has to be set up not only for the microscopic fermionic fields as in [49], but requires collective bosonic field variables, as introduced in the next section. As a side remark we note that continuation of the RG flow into regimes with broken symmetry can also be achieved in purely fermionic descriptions without Hubbard-Stratonovich transformation by inserting an infinitesimally small symmetry-breaking component in the initial action [84, 85].

The above mentioned regulator function  $R_k$  is to some extent arbitrary function, satisfying a few conditions for implementing a meaningful regularization [70, 73, 74]. Whereas exact solutions do not at all depend on the specific choice of  $R_k$ , approximate solutions and even estimates of universal (i.e., regularization scheme independent quantities) can depend on  $R_k$ . In the present work, we will use this variation of universal quantities as a function of  $R_k$  as an estimate for the systematic error introduced by our approximations. We consider results obtained for the *linear* regulator as our best estimate, as it satisfies RG optimization criteria [73, 86]. By contrast, the *sharp* cutoff is known to introduce strong regulator artifacts which we therefore use to maximally span the error bar for our approximations.

#### IV. LOW-ENERGY DEGREES OF FREEDOM

The partition function of the theory defined by (21),

$$Z = \int \mathcal{D}\bar{\chi}\mathcal{D}\chi \exp(-S), \quad (24)$$

is in fact equivalent to the partition function of the ‘‘mesonic’’ theory of a  $(2N_f) \times (2N_f)$  scalar matrix field  $\phi^{ij}$  and a vector field  $V_\mu$ , coupling via a Yukawa-type interaction to the fermions,

$$Z = \mathcal{N} \int \mathcal{D}\chi\mathcal{D}\bar{\chi}\mathcal{D}\phi\mathcal{D}V \exp \left[ - \left( \bar{\chi}^i i \not{\partial} \chi^i + \frac{1}{2} \bar{m}_\phi^2 \phi^{ij} \phi^{ji} + \frac{1}{2} \bar{m}_V^2 V_\mu^2 - \bar{h}_V V_\mu \bar{\chi}^i \sigma_\mu \chi^i + i \bar{h}_\phi \bar{\chi}^i \phi^{ij} \chi^j \right) \right], \quad (25)$$

where  $i, j = 1, \dots, 2N_f$ . The equivalence can be seen by multiplying Eq. (24) with appropriate Gaussian (Hubbard-Stratonovich) factors,

$$1 = \mathcal{N} \int \mathcal{D}\phi \exp \left[ -\frac{1}{2} \left( \bar{m}_\phi \phi^{ij} + i \frac{\bar{h}_\phi}{\bar{m}_\phi} \bar{\chi}^j \chi^i \right) \times \left( \bar{m}_\phi \phi^{ji} + i \frac{\bar{h}_\phi}{\bar{m}_\phi} \bar{\chi}^i \chi^j \right) \right], \quad (26)$$

$$1 = \mathcal{N} \int \mathcal{D}V \exp \left[ -\frac{1}{2} \left( \bar{m}_V V_\mu - \frac{\bar{h}_V}{\bar{m}_V} \bar{\chi}^i \sigma_\mu \chi^i \right)^2 \right], \quad (27)$$

with some normalization constants  $\mathcal{N}$ , not affecting any expectation values. The scalar matrix field is Hermitian,  $\phi^\dagger = \phi$ , and the vector field  $V$  is real. The four-fermi terms in Eq. (24) are then precisely canceled if the constraints

$$\frac{\bar{h}_\phi^2}{2\bar{m}_\phi^2} = \frac{\bar{g}_\phi}{2N_f}, \quad \frac{\bar{h}_V^2}{2\bar{m}_V^2} = \frac{\bar{g}_V}{2N_f}, \quad (28)$$

are imposed at the microscopic scale. From Eqs. (26)–(27) we can read off the properties of the boson fields under chiral transformations,

$$U(2N_f) : \quad \phi^{ij} \mapsto U^{ik} \phi^{kl} (U^\dagger)^{lj}, \quad V_\mu \mapsto V_\mu, \quad (29)$$

$U \in U(2N_f)$ . The scalar matrix  $\phi$  may be decomposed into a traceless part and its trace [87]

$$\Phi^{ij} := \phi^{ij} - \frac{\delta^{ij}}{2N_f} \text{Tr} \phi, \quad \varphi := \text{Tr} \phi. \quad (30)$$

The  $\varphi$  field is parity odd and can be attributed to the parity breaking channel ( $P$ )  $\sim \bar{\psi}^a \gamma_{45} \psi^a = \bar{\chi}^i \chi^i$ . By contrast, a vacuum expectation value of the traceless part  $\Phi$  corresponds to the dynamical breakdown of chiral symmetry,

$$\langle \Phi^{ij} \rangle \neq 0 \quad \Leftrightarrow \quad \langle \bar{\psi}^a \psi^a \rangle = \langle \bar{\chi}^a \chi^a - \bar{\chi}^{a+N_f} \chi^{a+N_f} \rangle \neq 0, \quad (31)$$

$a = 1, \dots, N_f$ , with the breaking pattern

$$U(2N_f) \rightarrow U(N_f) \otimes U(N_f). \quad (32)$$

We can trade the  $(2N_f) \times (2N_f)$  Hermitian traceless matrix  $\Phi$  for its independent components  $\Phi_\alpha$ ,

$$\Phi^{ij} = \sqrt{2} \Phi_\alpha (t_\alpha)^{ij}, \quad (33)$$

$i, j = 1, \dots, 2N_f$ ,  $\alpha = 1, \dots, (2N_f)^2 - 1$ , where the  $t_\alpha$  are the generators of  $SU(2N_f)$  in the fundamental representation, normalized so that  $\text{Tr}(t_\alpha t_\beta) = \delta_{\alpha\beta}/2$ .

In the one-flavor case  $N_f = 1$  this formulation is equivalent to a partial bosonization of the Fierz basis in the four-spinor representation (17): the Hubbard-Stratonovich transformation leads to the equivalent Yukawa-type theory with three scalar modes  $(\sigma, \tau, \pi) \sim (\bar{\psi}\psi, \bar{\psi}\gamma_4\psi, \bar{\psi}\gamma_5\psi)$  and a vector mode  $V_\mu \sim \bar{\psi}\gamma_\mu\psi$  with Lagrangian density

$$\mathcal{L}^{N_f=1} = \bar{\psi} i \not{\partial} \psi + \frac{1}{2} \bar{m}_\sigma^2 (\sigma^2 + \tau^2 + \pi^2) + i \bar{h}_\sigma \bar{\psi} (\sigma + i\gamma_4\tau + i\gamma_5\pi) \psi - \bar{h}_V V_\mu \bar{\psi} \gamma_\mu \psi. \quad (34)$$

From the discussion of the fermionic RG flow [49] we expect that the long-range dynamics of this system is dominated by the scalar NJL-type channel. For large enough coupling  $\bar{h}_\sigma^2/\bar{m}_\sigma^2$  we thus expect the scalar mode to acquire a nonvanishing vacuum expectation value (VEV), e.g., in the  $\sigma$  direction, and the spectrum in the broken phase consists of two massless Goldstone modes, e.g.,  $\tau$  and  $\pi$ , and a massive radial mode  $\sigma$ . The corresponding critical behavior is an interesting problem by itself: this system can be viewed as an effective low-energy theory of spinless electrons on the honeycomb lattice and thus as a simple model for suspended graphene [33]. It has also been studied in the context of magnetic catalysis [88]. In the following, we will focus on the case  $N_f > 1$  where a true competition between the two channels ( $V$ ) and ( $S$ ) is expected.

In contrast to the purely fermionic formulation [49], the bosonized formulation presented here is well suitable to quantitatively describe the spontaneous breaking of chiral symmetry. Loosely speaking, the bosonic fields  $\phi^{ij}$  and  $V_\mu$  parametrize the possible formation of bound states of the fermionic fields  $\sim \bar{\chi}^i \chi^j$  and  $\sim \bar{\chi}^i \sigma_\mu \chi^i$ , respectively. The corresponding critical phenomena of such a strongly-correlated system require nonperturbative approximation schemes. The functional renormalization group formulated in terms of the Wetterich equation is such an appropriate tool and has already shown its quantitative reliability in other (2+1)-dimensional relativistic fermion systems, see e.g., [55, 82, 83]. In the effective action we then have to take into account also higher boson-boson interactions generated through fluctuations, e.g.,

$$(\text{Tr} \Phi^2)^2 = (\Phi_\alpha \Phi_\alpha)^2, \quad (35)$$

$$\text{Tr} \Phi^4 = \frac{1}{2N_f} (\Phi_\alpha \Phi_\alpha)^2 + 2d_{\alpha\beta\epsilon} d_{\gamma\delta\epsilon} \Phi_\alpha \Phi_\beta \Phi_\gamma \Phi_\delta, \quad (36)$$

where the  $d_{\alpha\beta\gamma}$ 's are the structure constants for the group  $SU(2N_f)$ . For  $N_f = 1$  the  $d_{\alpha\beta\gamma}$ 's vanish. For computational reasons, we use the representation (25) for the case of general  $N_f$  with scalar matrix field  $\phi^{ij}$  having arbitrary trace.

We parameterize the dynamics of the low-energy degrees of freedom by an ansatz for the effective average action  $\Gamma_k$ . This ansatz corresponds to a systematic expansion of the action in powers of the field gradients to second order. Moreover, we simplify the discussion by considering interactions only up to fourth order in the fields. Our ansatz for the effective action then reads

$$\begin{aligned} \Gamma_k = \int_x & \left[ Z_{\chi,k} \bar{\chi}^i i \not{\partial} \chi^i + \frac{Z_{\phi,k}}{2} \partial_\mu \phi^{ij} \partial_\mu \phi^{ji} + U_k(\phi) \right. \\ & + \frac{Z_{V,k}}{4} V_{\mu\nu} V_{\mu\nu} + \frac{\bar{A}_{V,k}}{2} (\partial_\mu V_\mu)^2 + \frac{\bar{m}_{V,k}^2}{2} V_\mu V_\mu \\ & + \frac{\bar{\zeta}_k}{6} V_\mu V_\mu \partial_\nu V_\nu + \frac{\bar{\mu}_k}{8} (V_\mu V_\mu)^2 + \frac{\bar{\nu}_k}{4} V_\mu V_\mu \phi^{ij} \phi^{ji} \\ & - \bar{h}_{V,k} V_\mu \bar{\chi}^i \gamma_\mu \chi^i + i \bar{h}_{\phi,k} \bar{\chi}^i \phi^{ij} \chi^j \\ & \left. - \frac{\bar{g}_{V,k}}{2N_f} (\bar{\chi}^i \sigma_\mu \chi^i)^2 + \frac{\bar{g}_{\phi,k}}{2N_f} (\bar{\chi}^i \chi^j)^2 \right], \end{aligned} \quad (37)$$

where  $V_{\mu\nu} := \partial_\mu V_\nu - \partial_\nu V_\mu$  and  $i, j = 1, \dots, 2N_f$ .  $U_k(\phi)$  describes an effective potential in the scalar sector. All couplings in the effective action are understood to be scale-dependent, indicated by the index  $k$ . It is straightforward to match this action exactly to the microscopic models discussed above. For instance, by setting all bosonic couplings to zero at the UV cutoff scale  $k = \Lambda$ , we return to the fermionic action (21). Alternatively, we can set the fermionic couplings to zero,  $g_{V,\Lambda}, g_{\phi,\Lambda} = 0$ , and choose the compositeness conditions

$$Z_{\phi,k}, Z_{V,k}, \bar{A}_{V,k}, \bar{\zeta}_k \rightarrow 0, \quad \text{for } k \rightarrow \Lambda, \quad (38)$$

which guarantee that the bosonic fields have no kinetic term and are purely auxiliary at the high scale. Furthermore, satisfying the constraints (28) and setting the higher-order bosonic interactions to zero at  $k \rightarrow \Lambda$  leads us to the Yukawa-type theory as given in Eq. (25). This implements the Hubbard-Stratonovich transformation at a fixed scale  $k = \Lambda$  in the functional RG context. Of course, as soon as we start integrating out modes, the couplings set to zero at one scale can be generated at lower scales due to fluctuations. Also the constraints (28) will generally not be satisfied at lower scales. Whereas the purely fermionic flow has been extensively discussed in [49], we will now concentrate on the partially bosonized variants. We start with computing the RG flow in Sec. VI for the fixed-field variables introduced above. As the Hubbard-Stratonovich transformation demonstrates, the effective action (37) contains some redundancy, as field reparametrizations can trade various operators for one another. In Sec. VII, we exploit this redundancy to introduce scale-dependent fields that adjust the fermion-boson couplings dynamically in order

to effectively perform Hubbard-Stratonovich transformations on each scale (dynamical bosonization). In the following, we will mostly ignore the momentum-dependent terms in the vector channel, i.e., we will consider the pointlike limit

$$Z_{V,k} \rightarrow 0, \quad \bar{A}_{V,k} \rightarrow 0, \quad \bar{\zeta}_k \rightarrow 0, \quad \text{for all } k. \quad (39)$$

The beta functions will however be computed for general  $Z_{V,k}, \bar{A}_{V,k} \geq 0$  (but  $\bar{\zeta}_k = 0$ ).

## V. SCALAR MASS SPECTRUM

Due to  $U(2N_f)$  symmetry, the effective potential  $U_k(\phi)$  necessarily has to be a pure function of  $U(2N_f)$ -invariant quantities. The Hermitian scalar matrix field can be diagonalized by a  $U(2N_f)$  rotation [cf. Eq. (29)],

$$\phi \mapsto U \phi U^\dagger = \begin{pmatrix} \hat{m}_1 & 0 & \dots & 0 \\ 0 & \hat{m}_2 & \dots & 0 \\ \vdots & & \ddots & \vdots \\ 0 & 0 & \dots & \hat{m}_{2N_f} \end{pmatrix}, \quad (40)$$

with real eigenvalues  $\hat{m}_i$ . In a quartic approximation  $U_k(\phi)$  can then be parametrized in terms of the two invariants  $\rho$  and  $\tau$ ,

$$\rho = \frac{1}{2} \text{Tr} \phi^2 = \frac{1}{2} \sum_i \hat{m}_i^2, \quad (41)$$

$$\tau = \frac{1}{2} \text{Tr} \left( \frac{1}{2} \phi^2 - \frac{\rho}{2N_f} \right)^2 = \frac{1}{8} \sum_i \hat{m}_i^4 - \frac{1}{2} \left( \frac{\sum_i \hat{m}_i}{4N_f} \right)^2. \quad (42)$$

At higher field orders the potential can depend on additional (suitably defined [89]) higher order invariants constructed from  $\tilde{\tau}_n \sim \text{Tr}(\phi^2/2 - \rho/2N_f)^n$  for  $n \geq 3$ . We expand the scalar potential about its  $k$ -dependent minimum  $(\rho_{0,k}, \tau_{0,k})$ . In the symmetric (SYM) regime the potential is minimal at the origin  $(\rho_{0,k}, \tau_{0,k}) = (0, 0)$ , whereas in the chiral symmetry broken ( $\chi$ SB) regime we allow for a nonvanishing VEV which we assume to be acquired along the  $\rho$  direction, i.e.,  $\rho_{0,k} > 0$  and  $\tau_{0,k} = 0$ :

$$U_k(\rho, \tau) = \begin{cases} \bar{m}_{\phi,k}^2 \rho + \frac{\bar{\lambda}_{1,k}}{2} \rho^2 + \bar{\lambda}_{2,k} \tau, & \text{SYM regime,} \\ \frac{\bar{\lambda}_{1,k}}{2} (\rho - \rho_{0,k})^2 + \bar{\lambda}_{2,k} \tau, & \chi\text{SB regime.} \end{cases} \quad (43)$$

If the potential solely depends on  $\rho$  and  $\tau$ , it is sufficient to evaluate its flow equation in a two-dimensional subspace of all possible scalar configurations. We consider the traceless class, valid for  $N_f > 1$ ,

$$(\phi^{ij}) =: \hat{m} \text{diag}(\underbrace{\epsilon, +1, \dots, +1}_{N_f-1 \text{ times}}, \underbrace{-\epsilon, -1, \dots, -1}_{N_f-1 \text{ times}}), \quad (44)$$

TABLE I. Spectrum of the scalar mass matrix  $\delta^2 U_k / \delta\phi\delta\phi$  for  $\partial^2 U_k / \partial\tau^2 = \partial^2 U_k / \partial\rho\partial\tau = 0$  and  $N_f > 1$ . Primes denote partial derivatives with respect to  $\rho$ ,  $U_k^{(n)} \equiv \partial^n U_k / \partial\rho^n$ , and  $U_{k,\tau} \equiv \partial U_k / \partial\tau$ . For  $\hat{m} \equiv \hat{m}(\rho, \tau)$  and  $\epsilon \equiv \epsilon(\rho, \tau)$  see Eqs. (45)–(46).

Eigenvalue	Degeneracy
$U'_k + \frac{\hat{m}^2}{2} U_{k,\tau} \left[ 3\epsilon^2 - 1 + \frac{1-\epsilon^2}{N_f} \right]$	1
$U'_k + \frac{\hat{m}^2}{4N_f} \left\{ 4N_f(N_f - 1)U''_k + (4 - N_f)U_{k,\tau} + [4N_f U''_k + (3N_f - 4)U_{k,\tau}] \epsilon^2 \right.$ $\left. \pm \left[ (4N_f(N_f - 1)U''_k + (N_f + 2)U_{k,\tau})^2 \right. \right.$ $\left. + 2(16N_f^2(N_f - 1)U''_k{}^2 - 4N_f(N_f + 2)(3N_f - 2)U''_k U_{k,\tau} \right.$ $\left. - (3N_f^2 - 4N_f + 4)U_{k,\tau}^2 \right] \epsilon^2 + (4N_f U''_k + (3N_f - 2)U_{k,\tau})^2 \epsilon^4 \left. \right\}^{1/2}$	1 + 1
$U'_k + \frac{\hat{m}^2}{2} U_{k,\tau} \frac{1-N_f}{N_f} (1 - \epsilon^2)$	2
$U'_k + \frac{\hat{m}^2}{2} U_{k,\tau} \left[ \epsilon^2 \pm \epsilon + \frac{1-\epsilon^2}{N_f} \right]$	$4(N_f - 1) + 4(N_f - 1)$
$U'_k + \frac{\hat{m}^2}{2} U_{k,\tau} \left[ 2 + \frac{1-\epsilon^2}{N_f} \right]$	$2N_f^2 - 4N_f + 1$
$U'_k + \frac{\hat{m}^2}{2} U_{k,\tau} \frac{1-\epsilon^2}{N_f}$	$2(N_f - 1)^2$

where  $\epsilon \geq 1$ ,  $\hat{m} \in \mathbb{R}$ . For any  $\rho$  and  $\tau$  with  $\tau/\rho^2 < (N_f - 1)/4N_f$ , the parameters  $\hat{m}$  and  $\epsilon$  are given by

$$\hat{m}^2 = \frac{\rho}{N_f} \left( 1 - \sqrt{\frac{4N_f}{N_f - 1} \frac{\tau}{\rho^2}} \right), \quad (45)$$

$$\epsilon^2 = 1 + N_f \left( \frac{1}{1 - \sqrt{\frac{4N_f}{N_f - 1} \frac{\tau}{\rho^2}}} - 1 \right). \quad (46)$$

If the flow eventually chooses a vacuum configuration with  $\epsilon = 1$  and  $\hat{m} > 0$ , the chiral symmetry is spontaneously broken while parity symmetry remains preserved,

$$\left( \phi_0^{ij} \right) = \frac{\rho_0}{N_f} \begin{pmatrix} \mathbb{1} & 0 \\ 0 & -\mathbb{1} \end{pmatrix} \neq 0$$

$$\Leftrightarrow \langle \bar{\chi}^a \chi^a - \bar{\chi}^{a+N_f} \chi^{a+N_f} \rangle = \langle \bar{\psi}^a \psi^a \rangle \neq 0. \quad (47)$$

For simplicity, we assume in the following that  $\partial^2 U_k / \partial\tau^2 = \partial^2 U_k / \partial\rho\partial\tau = 0$ , which holds in the case of the quartic approximation (43). The spectrum of the scalar mass matrix  $\delta^2 U_k / \delta\phi\delta\phi$  for  $N_f > 1$  is given in Table I.

For a vacuum configuration with  $\epsilon = 1$  we have  $\tau_{0,k} = 0$ . In the SYM regime  $\rho_{0,k} = 0$ , all modes are degenerate and have mass  $\bar{m}_\phi^2 = \partial U_k / \partial\rho|_{(\rho,\tau)=(0,0)}$ . In the  $\chi$ SB regime with  $\rho_{0,k} > 0$  and  $\partial U_k / \partial\rho|_{(\rho,\tau)=(\rho_{0,k},0)} = 0$  we find  $2N_f^2$  massless scalar modes corresponding exactly to the number of broken generators in the symmetry breaking pattern

$$U(2N_f) \rightarrow U(N_f) \otimes U(N_f), \quad (48)$$

in accordance with Goldstone's theorem. Additionally, we obtain one massive radial mode with  $\bar{m}_\rho^2 = 2\rho_{0,k} \partial^2 U_k / \partial\rho^2$  and  $2N_f^2 - 1$  massive modes in  $\tau$  direction with  $\bar{m}_\tau^2 = (\rho_{0,k}/N_f) \partial U_k / \partial\tau$ . Since  $\delta\tau/\delta\phi|_{\phi_0} = 0$  we expect the  $2N_f^2 - 1$  degeneracy of the masses  $\bar{m}_\tau^2$  to

be a general result, holding also beyond our quartic approximation (43), as long as no higher-order invariants  $\sim \tilde{\tau}_n$  become important.

## VI. PARTIALLY BOSONIZED RG FLOW

Next, we determine the flow of the model in a partially bosonized description. This corresponds to start at the high scale with the Hubbard-Stratonovich transformed action of (25) and the compositeness condition (38). As is standard in this type of truncation, higher-order fermionic interactions are set to zero also on all lower scales.

We fix the standard RG invariance of field rescalings by defining the renormalized fields as

$$\tilde{\phi}^{ij} := Z_{\phi,k}^{1/2} \phi^{ij}, \quad \tilde{\chi}^i := Z_{\chi,k}^{1/2} \chi^i, \quad (49)$$

$$\tilde{V}_\mu := Z_{V,k}^{1/2} V_\mu, \quad \tilde{\chi}^i := Z_{\chi,k}^{1/2} \chi^i. \quad (50)$$

The dimensionless effective potential for space-time dimension  $d$  then reads

$$u(\tilde{\rho}, \tilde{\tau}) := k^{-d} U_k(Z_{\phi,k}^{-1} k^{d-2} \tilde{\rho}, Z_{\phi,k}^{-2} k^{2(d-2)} \tilde{\tau}), \quad (51)$$

where  $\tilde{\rho} := Z_{\phi,k} k^{2-d} \rho$  and  $\tilde{\tau} := Z_{\phi,k}^2 k^{2(2-d)} \tau$ , and the dimensionless renormalized couplings are

$$A_{V,k} := Z_V^{-1} \bar{A}_{V,k}, \quad \nu := Z_{\phi,k}^{-1} Z_{V,k}^{-1} k^{d-4} \bar{\nu}_k, \quad (52)$$

$$m_V^2 := Z_{V,k}^{-1} k^{-2} \bar{m}_{V,k}^2, \quad h_\phi^2 := Z_{\phi,k}^{-1} Z_{\chi,k}^{-2} k^{d-4} \bar{h}_{\phi,k}^2, \quad (53)$$

$$\mu := Z_{V,k}^{-2} k^{d-4} \bar{\mu}_k, \quad h_V^2 := Z_{V,k}^{-1} Z_{\chi,k}^{-2} k^{d-4} \bar{h}_{V,k}^2. \quad (54)$$

By evaluating the Wetterich equation (23) for a constant scalar background field (44), we obtain the flow of the

dimensionless scalar potential

$$\begin{aligned} \partial_t u &= -du + (d-2+\eta_\phi)\tilde{\rho}u' + (2d-4+2\eta_\phi)\tilde{\tau}u_{,\tilde{\tau}} \\ &+ 2v_d \sum_{i=1}^{2N_f} \ell_0^{(B)d}(m_i^2; \eta_\phi) + 2v_d d \ell_0^{(B)d}(m_V^2 + \nu\tilde{\rho}; \eta_V) \\ &- 4v_d d_\gamma \left[ (N_f - 1) \ell_0^{(F)d}(\tilde{m}^2 h_\phi^2; \eta_\chi) \right. \\ &\quad \left. + \ell_0^{(F)d}(\tilde{m}^2 \epsilon^2 h_\phi^2; \eta_\chi) \right] \end{aligned} \quad (55)$$

with  $u \equiv u(\tilde{\rho}, \tilde{\tau})$ ,  $u' \equiv \partial u / \partial \tilde{\rho}$ ,  $u_{,\tilde{\tau}} \equiv \partial u / \partial \tilde{\tau}$  and  $\tilde{m}^2 := Z_{\phi,k} k^{2-d} \hat{m}^2$ . The dimensionless scalar masses  $m_i^2 \equiv m_i^2(\tilde{\rho}, \tilde{\tau})$  can straightforwardly be deduced from Table I. We have further defined the anomalous dimensions

$$\eta_{\phi/\chi/V} = -\partial_t \ln Z_{\phi/\chi/V,k}. \quad (56)$$

The flow involves the threshold functions  $\ell_0^{(B/F)}(\dots)$ , which encode the details of the regularization scheme; their definitions and explicit forms for the linear and the sharp cutoff are listed in the Appendix. We have abbreviated  $v_d^{-1} = 2^{d+1} \pi^{d/2} \Gamma(d/2)$ , i.e.,  $v_3^{-1} = 8\pi^2$ . As discussed above, we work here with the two-component Weyl spinors such that the dimension of the gamma matrices is  $d_\gamma = 2$ . By suitable differentiation of Eq. (55) we obtain the flow of the scalar couplings occurring in

Eq. (43). In the SYM regime,

$$\partial_t m_\phi^2 = \partial_t u' \Big|_{(\tilde{\rho}, \tilde{\tau})=(0,0)}, \quad (57)$$

$$\partial_t \lambda_1 = \partial_t u'' \Big|_{(\tilde{\rho}, \tilde{\tau})=(0,0)}, \quad \partial_t \lambda_2 = \partial_t u_{,\tilde{\tau}} \Big|_{(\tilde{\rho}, \tilde{\tau})=(0,0)}, \quad (58)$$

whereas in the  $\chi$ SB regime,

$$\partial_t \kappa = -\frac{1}{\lambda_1} \partial_t u' \Big|_{(\tilde{\rho}, \tilde{\tau})=(\kappa,0)}, \quad (59)$$

$$\partial_t \lambda_1 = \partial_t u'' \Big|_{(\tilde{\rho}, \tilde{\tau})=(\kappa,0)}, \quad \partial_t \lambda_2 = \partial_t u_{,\tilde{\tau}} \Big|_{(\tilde{\rho}, \tilde{\tau})=(\kappa,0)}, \quad (60)$$

with the dimensionless VEV  $\kappa := Z_{\phi,k} k^{2-d} \rho_{0,k}$  and the abbreviations  $u^{(n)} \equiv \partial^n u / \partial \tilde{\rho}^n$  and  $u_{,\tilde{\tau}} \equiv \partial u / \partial \tilde{\tau}$ .

Similarly, the flow equations for all other couplings present in the effective action are straightforwardly obtained by suitable projections of the Wetterich equation (23). This amounts to a summation of all possible 1-loop diagrams where the vertices are given by full (though truncated) vertex functions and the inner lines correspond to the full propagators. With the useful Mathematica package DoFun [90], the evaluation of the RG flow equation can be automated easily. The beta function for the vector mass reads

$$\begin{aligned} \partial_t m_V^2 &= (-2 + \eta_V) m_V^2 - 2v_d (d+2) \ell_1^{(B)d}(m_V^2 + \nu\kappa; \eta_V) \mu \\ &- 2v_d \left[ 2N_f^2 \ell_1^{(B)d}(u'; \eta_\phi) + (2N_f^2 - 1) \ell_1^{(B)d}(u' + \frac{\kappa}{N_f} u_{,\tilde{\tau}}; \eta_\phi) + \ell_1^{(B)d}(u' + 2\kappa u''; \eta_\phi) \right] \nu \\ &+ \frac{8v_d (d-2) d_\gamma N_f}{d} \ell_1^{(F)d}(\frac{\kappa}{N_f} h_\phi^2; \eta_\chi) h_V^2 + \frac{16v_d d_\gamma}{d} \kappa \ell_2^{(F)d}(\frac{\kappa}{N_f} h_\phi^2; \eta_\chi) h_\phi^2 h_V^2, \end{aligned} \quad (61)$$

with the derivatives of the potential  $u^{(n)}$  and  $u_{,\tilde{\tau}}$  being evaluated at the minimum  $(\tilde{\rho}, \tilde{\tau}) = (\kappa, 0)$ . In the symmetric regime we have of course  $\kappa = 0$ . For the vector-vector interaction  $\mu$  and the vector-scalar interaction  $\nu$  we get

$$\begin{aligned} \partial_t \mu &= (d-4+2\eta_V)\mu + \frac{2v_d(d^2+10d+12)}{d+2} \ell_2^{(B)d}(m_V^2 + \nu\kappa; \eta_V) \mu^2 \\ &+ 2v_d \left[ 2N_f^2 \ell_2^{(B)d}(u'; \eta_\phi) + (2N_f^2 - 1) \ell_2^{(B)d}(u' + \frac{\kappa}{N_f} u_{,\tilde{\tau}}; \eta_\phi) + \ell_2^{(B)d}(u' + 2\kappa u''; \eta_\phi) \right] \nu^2 \\ &+ \frac{16v_d(d-2)(4-d) d_\gamma N_f}{d(d+2)} \ell_2^{(F)d}(\frac{\kappa}{N_f} h_\phi^2; \eta_\chi) h_V^4 + \frac{128v_d(4-d) d_\gamma}{d(d+2)} \kappa \ell_3^{(F)d}(\frac{\kappa}{N_f} h_\phi^2; \eta_\chi) h_\phi^2 h_V^4 \\ &- \frac{384v_d d_\gamma}{d(d+2) N_f} \kappa^2 \ell_4^{(F)d}(\frac{\kappa}{N_f} h_\phi^2; \eta_\chi) h_\phi^4 h_V^4, \end{aligned} \quad (62)$$

$$\begin{aligned}
\partial_t \nu &= (d-4 + \eta_\phi + \eta_V) \nu + 2(d+2)v_d \ell_2^{(B)d} (m_V^2 + \nu\kappa; \eta_V) \mu\nu \\
&+ v_d \left\{ \left( \frac{2N_f^2 + 1}{N_f^2} u'' + \frac{2N_f^2 - 1}{2N_f^3} u, \bar{\tau} \right) \left[ 2N_f^2 \ell_2^{(B)d} (u'; \eta_\phi) + (2N_f^2 - 1) \ell_2^{(B)d} (u' + \frac{\kappa}{N_f} u, \bar{\tau}; \eta_\phi) \right. \right. \\
&\quad \left. \left. + \ell_2^{(B)d} (u' + 2\kappa u''; \eta_\phi) \right] + \frac{1}{N_f} u, \bar{\tau} \ell_2^{(B)d} (u' + \frac{\kappa}{N_f} u, \bar{\tau}; \eta_\phi) \right\} \nu \\
&+ \frac{2v_d}{N_f^2} \left[ 2N_f^2 \ell_{1,1}^{(BB)d} (u', m_V^2 + \nu\kappa; \eta_\phi, \eta_V) + (2N_f^2 - 1) \ell_{1,1}^{(BB)d} (u' + \frac{\kappa}{N_f} u, \bar{\tau}, m_V^2 + \nu\kappa; \eta_\phi, \eta_V) \right. \\
&\quad \left. + \ell_{1,1}^{(BB)d} (u' + 2\kappa u'', m_V^2 + \nu\kappa; \eta_\phi, \eta_V) \right] \nu^2 + \frac{8v_d(4-d)d_\gamma}{d} \ell_2^{(F)d} (\frac{\kappa}{N_f} h_\phi^2; \eta_\chi) h_V^2 h_\phi^2 \\
&- \frac{96v_d d_\gamma}{dN_f} \kappa \ell_3^{(F)d} (\frac{\kappa}{N_f} h_\phi^2; \eta_\chi) h_V^2 h_\phi^4 - \frac{32v_d(4-d)d_\gamma}{dN_f^2} \kappa^2 \ell_4^{(F)d} (\frac{\kappa}{N_f} h_\phi^2; \eta_\chi) h_V^2 h_\phi^6. \tag{63}
\end{aligned}$$

In the symmetric regime the flow of the Yukawa coupling  $h_\phi$  is unambiguous. In the broken regime however the diverse scalar modes in general can develop different couplings. We will focus on the Goldstone-mode coupling to the fermions, which is expected to give the dominant contribution for aspects of criticality. However, this Goldstone-mode projection may introduce artifacts deeply in the broken regime, see below. The flow equation reads

$$\begin{aligned}
\partial_t h_\phi^2 &= (d-4 + \eta_\phi + 2\eta_\chi) h_\phi^2 \\
&+ \frac{4v_d}{N_f} \left[ \ell_{1,1}^{(FB)d} (\frac{\kappa}{N_f} h_\phi^2, u' + \frac{\kappa}{N_f} u, \bar{\tau}; \eta_\chi, \eta_\phi) - \ell_{1,1}^{(FB)d} (\frac{\kappa}{N_f} h_\phi^2, u' + 2\kappa u''; \eta_\chi, \eta_\phi) \right] h_\phi^4 \\
&+ \frac{8v_d}{N_f^2} \kappa \left[ 2N_f^2 u'' \ell_{1,2}^{(FB)d} (\frac{\kappa}{N_f} h_\phi^2, u'; \eta_\chi, \eta_\phi) + ((2N_f^2 - 1)u, \bar{\tau} + 2(N_f - 1)u'') \ell_{1,1,1}^{(FBB)d} (\frac{\kappa}{N_f} h_\phi^2, u', u' + \frac{\kappa}{N_f} u, \bar{\tau}; \eta_\chi, \eta_\phi) \right. \\
&\quad \left. + (2u'' + u, \bar{\tau}) \ell_{1,1,1}^{(FBB)d} (\frac{\kappa}{N_f} h_\phi^2, u', u' + 2\kappa u''; \eta_\chi, \eta_\phi) \right] h_\phi^4 - 8v_d \ell_{1,1}^{(FB)d} (\frac{\kappa}{N_f} h_\phi^2, m_V^2 + \nu\kappa; \eta_\chi, \eta_V) h_\phi^2 h_V^2. \tag{64}
\end{aligned}$$

For the flow of the fermion-vector coupling we find

$$\begin{aligned}
\partial_t h_V^2 &= (d-4 + \eta_V + 2\eta_\chi) h_V^2 \\
&- \frac{4v_d(d-2)}{dN_f} \left[ 2N_f^2 \ell_{1,1}^{(FB)d} (\frac{\kappa}{N_f} h_\phi^2, u'; \eta_\chi, \eta_\phi) + (2N_f^2 - 1) \ell_{1,1}^{(FB)d} (\frac{\kappa}{N_f} h_\phi^2, u' + \frac{\kappa}{N_f} u, \bar{\tau}; \eta_\chi, \eta_\phi) \right. \\
&\quad \left. + \ell_{1,1}^{(FB)d} (\frac{\kappa}{N_f} h_\phi^2, u' + 2\kappa u''; \eta_\chi, \eta_\phi) \right] h_\phi^2 h_V^2 \\
&- \frac{8v_d}{dN_f^2} \kappa \left[ 2N_f^2 \ell_{2,1}^{(FB)d} (\frac{\kappa}{N_f} h_\phi^2, u'; \eta_\chi, \eta_\phi) + (2N_f^2 - 1) \ell_{2,1}^{(FB)d} (\frac{\kappa}{N_f} h_\phi^2, u' + \frac{\kappa}{N_f} u, \bar{\tau}; \eta_\chi, \eta_\phi) \right. \\
&\quad \left. + \ell_{2,1}^{(FB)d} (\frac{\kappa}{N_f} h_\phi^2, u' + 2\kappa u''; \eta_\chi, \eta_\phi) \right] h_\phi^4 h_V^2 \\
&- \frac{8v_d(d-2)^2}{d} \ell_{1,1}^{(FB)d} (\frac{\kappa}{N_f} h_\phi^2, m_V^2 + \nu\kappa; \eta_\chi, \eta_V) h_V^4 - \frac{16v_d(d-2)}{dN_f} \kappa \ell_{2,1}^{(FB)d} (\frac{\kappa}{N_f} h_\phi^2, m_V^2 + \nu\kappa; \eta_\chi, \eta_V) h_\phi^2 h_V^4, \tag{65}
\end{aligned}$$

and the anomalous dimensions read

$$\begin{aligned}
\eta_\phi &= \frac{8v_d d_\gamma}{d} m_4^{(F)d} (\frac{\kappa}{N_f} h_\phi^2; \eta_\chi) h_\phi^2 + \frac{8v_d d_\gamma}{dN_f} \kappa m_2^{(F)d} (\frac{\kappa}{N_f} h_\phi^2; \eta_\chi) h_\phi^4 \\
&+ \frac{16v_d}{dN_f^2} \kappa [N_f^2 u''^2 + (N_f - 1)u, \bar{\tau}^2] m_{2,2}^{(B)d} (u', u' + 2\kappa u''; \eta_\phi), \tag{66}
\end{aligned}$$

$$\begin{aligned}
\eta_\chi &= \frac{4v_d}{dN_f} \left[ 2N_f^2 m_{1,2}^{(FB)d} (\frac{\kappa}{N_f} h_\phi^2, u'; \eta_\chi, \eta_\phi) + (2N_f^2 - 1) m_{1,2}^{(FB)d} (\frac{\kappa}{N_f} h_\phi^2, u' + \frac{\kappa}{N_f} u, \bar{\tau}; \eta_\chi, \eta_\phi) \right. \\
&\quad \left. + m_{1,2}^{(FB)d} (\frac{\kappa}{N_f} h_\phi^2, u' + 2\kappa u''; \eta_\chi, \eta_\phi) \right] h_\phi^2 - 8v_d m_{1,2}^{(FB)d} (\frac{\kappa}{N_f} h_\phi^2, m_V^2 + \nu\kappa; \eta_\chi, \eta_V) h_V^2, \tag{67}
\end{aligned}$$

$$\eta_V = \frac{16v_d(d-2)d_\gamma N_f}{d} m_4^{(F)d} (\frac{\kappa}{N_f} h_\phi^2; \eta_\chi) h_V^2 + 16v_d d_\gamma \kappa m_2^{(F)d} (\frac{\kappa}{N_f} h_\phi^2; \eta_\chi) h_\phi^2 h_V^2. \tag{68}$$

---

Within our truncation we find that the flows of the two possible vector-field kinetic terms are in fact equivalent,

i.e.,  $\partial_t \bar{A}_k = \partial_t Z_{V,k}$ . The vector propagator thus is diagonal,  $G_{\mu\nu,k}^{(V)} = \delta_{\mu\nu} / (Z_{V,k} p^2 + \bar{m}_{V,k}^2)$ . The definitions of the threshold functions  $\ell_{\dots}^{(B/F)d}(\dots)$  and  $m_{\dots}^{(B/F)d}(\dots)$  are listed in the Appendix, together with their explicit forms for linear and sharp cutoff. The flow equations have been independently verified for the symmetric regime in local potential approximation with the DoFun package [90].

As is the case in the fermionic formulation, we expect the flow to be dominated by the vector channel for sufficiently large flavor number  $N_f$ . Whether for large coupling the  $V$  field then can develop a finite vacuum expectation value is an interesting question on its own right: e.g., (2+1)-dimensional models exhibiting spontaneous breaking of Lorentz symmetry have been investigated in [91–95]. By contrast, one could suspect that the vector mass eventually flows to zero, triggering a close resemblance of the strongly coupled Thirring model for large flavor number to a  $U(1)$  gauge theory. This is in fact the prediction of the large- $N_f$  studies [21, 96]. In the present work, we are mainly interested in a possible scalar condensation corresponding to chiral symmetry breaking and thus leave this issue for future studies.

As long as the vector mass  $m_V^2$  does not become too small it is then sufficient to consider the pointlike approximation in the vector channel,  $Z_{V,k} \rightarrow 0$ , corresponding to  $m_V^2 \rightarrow \infty$ . In this limit, the beta functions no longer depend on  $h_V^2$  and  $m_V^2$  separately but only on the ratio  $g_V = N_f h_V^2 / m_V^2$ , reflecting the RG invariance of fields rescalings. In the remaining flow equations the vector anomalous dimension  $\eta_V$  completely drops out. The flow of  $Z_{\chi,k}$  given by Eq. (67) is driven by a competition between a positive scalar loop term  $\propto h_\phi^2$  and a negative vector loop term  $\propto h_V^2$ . In the pointlike approximation of the vector sector,  $m_V^2 \rightarrow \infty$  and hence the vector loop term vanishes. For reasons of consistency, we will therefore suppress also the scalar loop term in Eq. (67), i.e., we treat the fermionic sector in the leading-order derivative approximation  $\eta_\chi \equiv 0$ . This is compatible with the observation that the flow of the fermionic wave function renormalization in 3d fermion systems at criticality is usually very small [55, 82, 83, 97–99]. As we shall see in Sec. VII, this assumption is exactly fulfilled for large number of fermion flavors  $N_f \rightarrow \infty$ , where the fixed-point equations can be solved analytically; in fact, this is the known result of the  $1/N_f$  expansion [20].

In comparison, the scalar anomalous dimension is nonvanishing in this limit, and we thus expect the flow of  $Z_{\phi,k}$  to be crucial also for finite  $N_f$ . We note that similar observations have also been made in other Yukawa-type systems in three dimensions, where a nonvanishing  $\eta_\phi \sim \mathcal{O}(1)$  is essential in order to find the correct critical behavior [55, 82, 83, 99]. Also the recent results for the  $N_f = 1$  model [33] fit into this scheme.

For the remainder of this section, we omit the vector-vector interaction  $\mu$  and the vector-scalar interaction  $\nu$  for simplicity. We concentrate on the UV structure only in order to compare it with our previous results

in the fermionic language. A full analysis of the IR properties of the dynamically bosonized RG flow follows in Sec. VII. For the search of a fixed point, we hence end up with a system of six coupled nonlinear equations for the five couplings in the SYM regime  $(m_\phi^2, \lambda_1, \lambda_2, h_\phi^2, N_f h_V^2 / m_V^2)$  and the anomalous dimension  $\eta_\phi$ . The stability matrix  $\partial \beta_i / \partial g_j |_{g^*}$  at a fixed point  $g^* = (m_\phi^{*2}, \lambda_1^*, \lambda_2^*, h_\phi^{*2}, N_f h_V^{*2} / m_V^{*2})$  has five eigenvalues, which we refer to as  $-\Theta_1, \dots, -\Theta_5$ , in ascending order according to their real part. In the large- $N_f$  limit the fixed-point structure can be mapped out analytically and we discover precisely the known structure from the fermionic flow [49]: the Thirring universality class is governed by a UV fixed point having one IR relevant direction with critical exponent  $\Theta_1 = 1$  and  $\Theta_{i \geq 2} < 0$ . It is located in the pure fermion-vector sector, i.e.,  $N_f h_\phi^{*2} / m_\phi^{*2} = 0$  and  $N_f h_V^{*2} / m_V^{*2} > 0$ . Moreover, the fixed-point position exactly coincides with the Thirring fixed point in the fermionic RG [49],

$$g_\phi^* = N_f \frac{h_\phi^{*2}}{m_\phi^{*2}} = 0, \quad \text{for } N_f \rightarrow \infty, \quad (69)$$

$$g_V^* = N_f \frac{h_V^{*2}}{m_V^{*2}} = \frac{3\pi^2}{2 \ell_1^{(F)}(0)}, \quad \text{for } N_f \rightarrow \infty, \quad (70)$$

for the dimensionless renormalized fermionic couplings  $g_\phi = Z_\chi^{-2} k^{d-2} \bar{g}_\phi$  and  $g_V = Z_\chi^{-2} k^{d-2} \bar{g}_V$ . For finite  $N_f$  we discover deviations from the fermionic fixed-point structure. In Fig. 4, results from the bosonized description are shown as black lines, and the corresponding fermionic results from [49] are plotted as gray lines. These deviations are not unexpected, since the fermionic description differs from the partially bosonized description in two respects: first, the fluctuation-induced kinetic terms of the bosons describe momentum-dependencies of the fermionic four-point functions. These momentum-dependencies are neglected in a fermionic derivative expansion used in [49]. In addition to this advantage of the partially bosonized description, there is also a disadvantage arising from the fact that the fluctuations are no longer Fierz-complete in the partially bosonized description even in the pointlike limit, as will be demonstrated explicitly in the next section.

The question which description is quantitatively more accurate cannot be answered a priori. There are, however, a couple of indications that the fermionic description is more reliable at least in the UV: First, as already observed in [49], the universal aspects of the UV fixed-point structure in the fermionic language do not depend on the choice of regulator, as it should be. If momentum-dependencies were important, we would expect a strong scheme dependence of the universal observables on approximate RG calculations. This UV stability of fermionic flows has been observed in a variety of contexts [100, 101]. Second, the fixed-point properties in the fermionic and partially bosonized description differ both quantitatively and qualitatively, as is visible in Fig. 4 for the Thirring fixed point. Also, in the bosonized language,

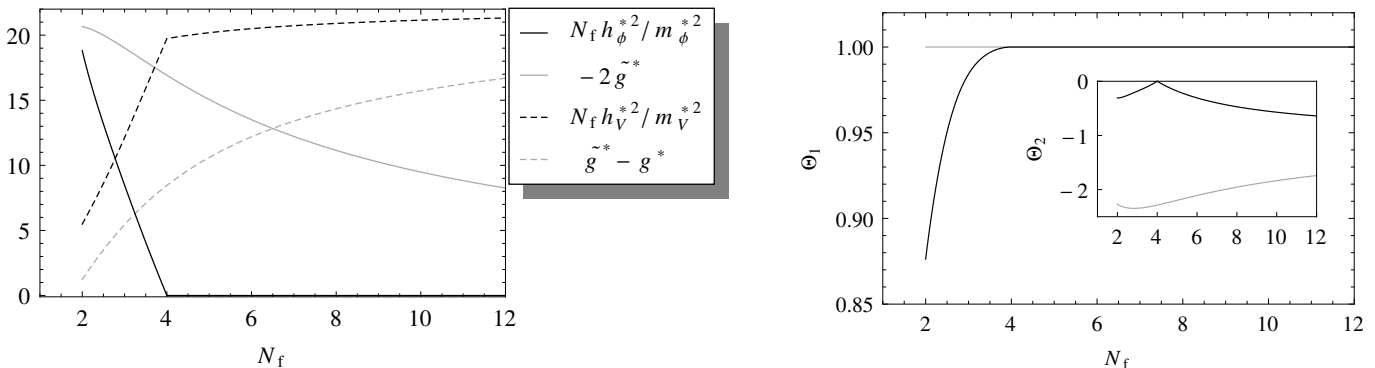


FIG. 4. Left panel: nonuniversal UV fixed-point values of the Thirring fixed point for the bosonic (black) and fermionic RG flow (gray, compiled from [49]) for the linear regulator. In the bosonic language already for  $N_f \geq 4$  the fixed point is located in the pure fermion-vector sector, while in the fermionic language this is the case only for large  $N_f$ . Fermionic and bosonic descriptions coincide only for  $N_f \rightarrow \infty$  but approach each other again for small  $N_f$ . Right panel: largest critical exponent  $\Theta_1$  and subleading exponent  $\Theta_2$  (inset).

we find two further interacting fixed points with two or more relevant directions (while there is only one fixed point with two relevant directions in the fermionic description). In fact, we observe a qualitative breakdown of the partially bosonized description for intermediate  $N_f$ : for  $N_f < 4$  the additional fixed points are located in the pure fermion-scalar sector  $h_V^2/m_V^2 = 0$  and the pure fermion-vector sector  $h_\phi^2/m_\phi^2 = 0$ , respectively. Since  $\partial_t h_\phi^2 \propto \mathcal{O}(h_\phi^2)$  and  $\partial_t h_V^2 \propto \mathcal{O}(h_V^2)$  both sectors are in fact invariant under RG transformations.

The Thirring fixed point, which for  $N_f < 4$  has components in both sectors,  $h_\phi^2/m_\phi^2 > 0$  and  $h_V^2/m_V^2 > 0$ , hits the fixed point in the pure fermion-vector sector once  $N_f \rightarrow 4$ . The fixed-point position as a function of  $N_f$  is therefore nonanalytic at  $N_f = 4$ . For  $N_f > 4$  the Thirring fixed-point stays in the fermion-vector subspace  $h_\phi^2/m_\phi^2 = 0$ , coinciding with the fermionic-RG fixed point only for  $N_f \rightarrow \infty$ . In Fig. 4 we have plotted the critical exponents for the RG relevant ( $\Theta_1$ ) and the RG irrelevant direction ( $\Theta_2$ ), showing good agreement in the former case while in the latter case, in particular for small  $N_f$ , large deviations occur.

To summarize: for large  $N_f \gg 1$ , we find a qualitative behavior which is consistent between the fermionic and the partially bosonized description. The scalar sector decouples for  $N_f \gg 1$  and only the fermion-vector interactions  $N_f h_V^2/m_V^2 \sim -g$  matter. For smaller  $N_f$ , the quantitative deviations between both descriptions increase and particularly the fixed-point structure becomes rather different, culminating at a nonanalyticity at  $N_f = 4$ . We interpret this behavior as a breakdown of the partially bosonized description arising from the Fierz incompleteness as shown below. Incidentally, the agreement between both descriptions improves again for smaller  $N_f$ , where the flow in both cases is dominated by a strong fermion-scalar coupling  $N_f h_\phi^2/m_\phi^2 \sim -2\tilde{g}$ . This single-channel dominance appears to alleviate the problem of Fierz incompleteness. This observation also

lends support to the recent single-channel analysis of the  $N_f = 1$  system [33].

We conclude that the ‘‘Fierz ambiguity’’ is a severe problem for partially bosonized formulations of the Thirring model precisely in the region where different channels compete with each other. For the location of the quantum phase transition in terms of a critical fermion number, a solution of this problem is mandatory. For applications of the Thirring model at a fixed given fermion number, say  $N_f = 2$  for graphene, a solution of this problem may still exert a sizable quantitative influence. A solution in terms of a dynamically bosonized RG flow will be presented in the next section.

## VII. DYNAMICALLY BOSONIZED RG FLOW

Although the bosonic partition function (25) is fully equivalent to the original fermion theory (21), the corresponding leading-order truncations of the effective action are not. The reason is that the four-fermi couplings, though absent in the bare action due to the Hubbard-Stratonovich trick, are again generated by the box diagrams displayed in Fig. 5. However, an inclusion of  $\bar{g}_{\phi,k}$  and  $\bar{g}_{V,k}$  in the truncation (37) does not seem very appealing, as it introduces a redundancy in the effective action. Instead, we employ dynamical bosonization [67, 73, 74, 102] as it has already been successfully used to resolve mean-field ambiguities [66] or implement particle-hole fluctuations in ultracold fermi gases [103]. Here we use the simplified approach<sup>2</sup> proposed in [67]. The idea is to perform a Hubbard-Stratonovich transformation at *each* RG step, such that all newly generated four-fermi

<sup>2</sup> This approach follows from an approximation to an exact equation [73] where the neglected terms are parametrically suppressed for the present application [74].

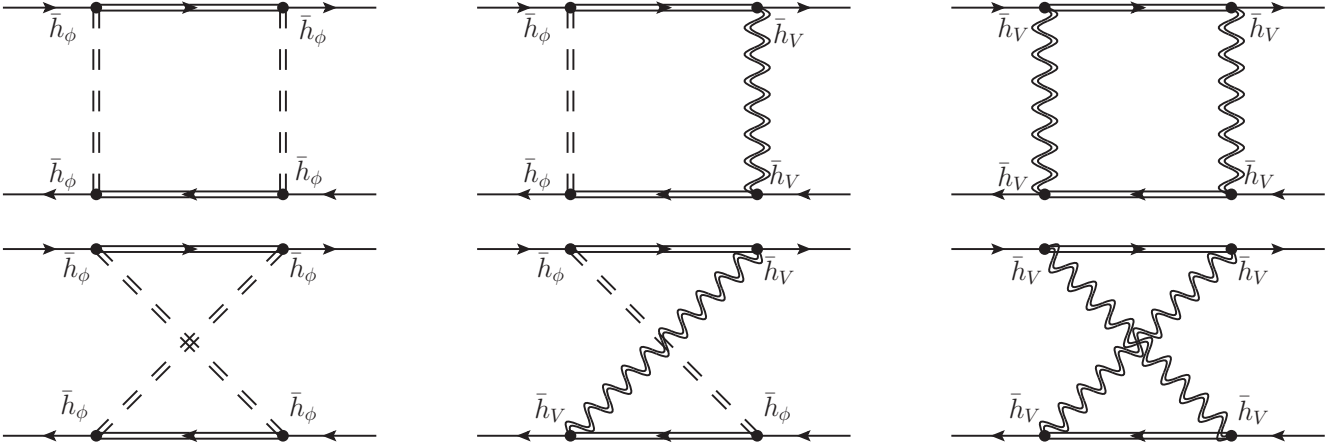


FIG. 5. Box diagrams contributing to the flow of  $g_\phi$  and  $g_V$ . Solid lines are fermions, dashed lines are scalar fields, and wiggly lines vector fields. Doubled inner lines denote full propagators  $G_k = (\Gamma_{k,0}^{(2)} + R_k)^{-1}$ .

interactions are again reexpressed in terms of the bosonic interactions. In this way, the four-fermi couplings  $\bar{g}_{\phi,k}$  and  $\bar{g}_{V,k}$  vanish at all scales. The bosonic fields then necessarily become scale dependent. We use the follow-

ing field redefinitions

$$\phi_{k-dk}^{ij} = \phi_k^{ij} - i(\bar{\chi}^j \chi^i) \delta\omega_{\phi,k}, \quad \phi_\Lambda \equiv \phi, \quad (71)$$

$$V_{\mu,k-dk} = V_{\mu,k} + (\bar{\chi}^i \sigma_\mu \chi^i) \delta\omega_{V,k}, \quad V_\Lambda \equiv V, \quad (72)$$

with to be determined functions  $\omega_{\phi/V,k}$ . Note that we keep the fermion fields fixed. For scale-dependent bosonic fields the flow equation for the effective average action is modified,

$$\begin{aligned} \partial_k \Gamma_k[\phi_k, V_k] &= \partial_k \Gamma_k[\phi_k, V_k] \Big|_{\phi_k, V_k} + \int \frac{\delta \Gamma_k[\phi_k, V_k]}{\delta \phi_k^{ij}} \partial_k \phi_k^{ij} + \int \frac{\delta \Gamma_k[\phi_k, V_k]}{\delta V_{\mu,k}} \partial_k V_{\mu,k} \\ &= \frac{1}{2} \text{STr} \frac{\partial_k R_k}{\Gamma_k^{(2)}[\phi_k, V_k] + R_k} + i \int \frac{\delta \Gamma_k[\phi_k, V_k]}{\delta \phi_k^{ij}} (\bar{\chi}^j \chi^i) \partial_k \omega_{\phi,k} - \int \frac{\delta \Gamma_k[\phi_k, V_k]}{\delta V_{\mu,k}} (\bar{\chi}^i \sigma_\mu \chi^i) \partial_k \omega_{V,k}, \end{aligned} \quad (73)$$

where the first term is evaluated for fixed fields and hence leads to the standard flow of  $\Gamma_k$  with  $\phi_\Lambda$  and  $V_\Lambda$  replaced by  $\phi_k$  and  $V_k$ , respectively [67]. We have suppressed the additional dependence of  $\Gamma_k$  on the fermion fields  $\bar{\chi}$  and  $\chi$  for brevity. Projecting onto the boson couplings, we find the beta functions

$$\partial_t u = \partial_t u \Big|_{\phi_k, V_k}, \quad \partial_t \nu^2 = \partial_t \nu^2 \Big|_{\phi_k, V_k}, \quad (74)$$

$$\partial_t m_V^2 = \partial_t m_V^2 \Big|_{\phi_k, V_k}, \quad \partial_t h_\phi^2 = \partial_t h_\phi^2 \Big|_{\phi_k, V_k} + u' \partial_t \omega_{\phi,k}, \quad (75)$$

$$\partial_t \mu^2 = \partial_t \mu^2 \Big|_{\phi_k, V_k}, \quad \partial_t h_V^2 = \partial_t h_V^2 \Big|_{\phi_k, V_k} + m_V^2 \partial_t \omega_{V,k}, \quad (76)$$

i.e., the scale-dependent bosonization changes only the flow of  $h_\phi^2$  and  $h_V^2$  and leaves the other beta functions in the bosonic sector invariant. For the four-fermi couplings

we obtain

$$\partial_t g_\phi = \partial_t g_\phi \Big|_{\phi_k, V_k} - h_\phi \partial_t \omega_{\phi,k}, \quad (77)$$

$$\partial_t g_V = \partial_t g_V \Big|_{\phi_k, V_k} - h_V \partial_t \omega_{V,k}. \quad (78)$$

Choosing

$$\partial_t \omega_{\phi,k} \equiv \frac{\beta_{g_\phi}}{h_\phi}, \quad \partial_t \omega_{V,k} \equiv \frac{\beta_{g_V}}{h_V}, \quad (79)$$

where  $\beta_{g_\phi} := \partial_t g_\phi \Big|_{\phi_k, V_k}$ ,  $\beta_{g_V} := \partial_t g_V \Big|_{\phi_k, V_k}$ , establishes that  $g_{V,k}$  and  $g_{\phi,k}$  vanish at all scales, if absent at the UV scale  $k = \Lambda$ . The beta functions  $\beta_{g_\phi}$  and  $\beta_{g_V}$  are straightforwardly obtained by suitable projections of the box diagrams in Fig. 5,

$$\begin{aligned}
\beta_{g_{\phi/V}} = & 4v_d a_{\phi/V}^{(1)} \left[ 2N_f^2 \ell_{1,2}^{(\text{FB})d} \left( \frac{\kappa}{N_f} h_\phi^2, u'; \eta_\chi, \eta_\phi \right) + (2N_f^2 - 1) \ell_{1,2}^{(\text{FB})d} \left( \frac{\kappa}{N_f} h_\phi^2, u' + \frac{\kappa}{N_f} u, \bar{\tau}; \eta_\chi, \eta_\phi \right) \right. \\
& \left. + \ell_{1,2}^{(\text{FB})d} \left( \frac{\kappa}{N_f} h_\phi^2, u' + 2\kappa u''; \eta_\chi, \eta_\phi \right) \right] h_\phi^4 + 4v_d a_{\phi/V}^{(2)} \ell_{1,2}^{(\text{FB})d} \left( \frac{\kappa}{N_f} h_\phi^2, m_V^2 + \nu\kappa; \eta_\chi, \eta_V \right) h_V^4 \\
& + 4v_d a_{\phi/V}^{(3)} \left[ 2N_f^2 \ell_{1,1,1}^{(\text{FBB})d} \left( \frac{\kappa}{N_f} h_\phi^2, u', m_V^2; \eta_\chi, \eta_\phi \right) + (2N_f^2 - 1) \ell_{1,1,1}^{(\text{FBB})d} \left( \frac{\kappa}{N_f} h_\phi^2, u' + \frac{\kappa}{N_f} u, \bar{\tau}, m_V^2; \eta_\chi, \eta_\phi \right) \right. \\
& \left. + \ell_{1,1,1}^{(\text{FBB})d} \left( \frac{\kappa}{N_f} h_\phi^2, u' + 2\kappa u'', m_V^2; \eta_\chi, \eta_\phi \right) \right] h_\phi^2 h_V^2 \quad (80)
\end{aligned}$$

with to be determined (possibly  $N_f$ -dependent) constants  $a_{\phi/V}^{(i)}$ . In the  $\chi$ SB regime the fermions couple also to the expectation value  $\kappa$  and there are more terms  $\sim \kappa \ell_{2,2}^{(\text{FB})d} (\kappa h_\phi^2 / N_f, \dots) h_{\phi/V}^4 h_\phi^2$ . They are suppressed for small  $\kappa \ll 1$  and bounded from above for large  $\kappa \gg 1$  since  $\kappa \ell_{2,2}^{(\text{FB})d}(\dots) \sim \kappa / (1 + \kappa h_\phi / N_f) \cdot \ell_{1,2}^{(\text{FB})d}(\dots)$ . We expect that such terms do not take a significant influence on the flow. For simplicity, we will omit them in the following. Instead of evaluating the diagrams in Fig. 5 explicitly, we can determine the  $a_{\phi/V}^{(i)}$  by taking advantage of the fact [66, 67] that the dynamically bosonized flow in the pointlike limit  $Z_{V,k} \rightarrow 0$  and  $Z_{\phi,k} \rightarrow 0$  exactly coincides with the fermionic flow computed in [49],

$$\partial_t \left( N_f \frac{h_\phi^2}{m_\phi^2} \right) \equiv -2\partial_t \tilde{g} \Big|_{\phi_k, V_k}, \quad (81)$$

$$\partial_t \left( N_f \frac{h_V^2}{m_V^2} \right) \equiv \partial_t (\tilde{g} - g) \Big|_{\phi_k, V_k}. \quad (82)$$

This fixes  $a_{\phi/V}^{(i)}$  uniquely and establishes an exact mapping of the fermionic fixed-point structure [49] onto the bosonized language in the pointlike limit. Beyond the pointlike approximation, the bosonized RG permits to reliably run toward and into the  $\chi$ SB regime, allowing us to predict the desired IR values of, for instance, fermion mass or order parameter as a function of  $N_f$ .

### VIII. UV STRUCTURE AND FIXED POINTS

#### A. Large- $N_f$ limit

In the limit of infinite flavor number  $N_f \rightarrow \infty$ , the flow equations simplify considerably. For the dynamically bosonized flow in the symmetric regime we have

$$\partial_t \left( \frac{m_\phi^2}{N_f^2} \right) = (-2 + \eta_\phi) \left( \frac{m_\phi^2}{N_f^2} \right), \quad (83)$$

$$\partial_t m_V^2 = (-2 + \eta_V) m_V^2 + \frac{2}{3\pi^2} \ell_1^{(\text{F})}(0; \eta_\chi) (N_f h_V^2), \quad (84)$$

$$\partial_t (N_f \lambda_1) = (-1 + 2\eta_\phi) (N_f \lambda_1) - \frac{1}{\pi^2} \ell_2^{(\text{F})}(0; \eta_\chi) h_\phi^4, \quad (85)$$

$$\partial_t \lambda_2 = (-1 + 2\eta_\phi) \lambda_2 - \frac{2}{\pi^2} \ell_2^{(\text{F})}(0; \eta_\chi) h_\phi^4, \quad (86)$$

$$\begin{aligned} \partial_t (N_f \mu) = & (-1 + 2\eta_V) (N_f \mu) \\ & + \frac{4}{15\pi^2} \ell_2^{(\text{F})}(0; \eta_\chi) (N_f h_V^2)^2, \end{aligned} \quad (87)$$

$$\begin{aligned} \partial_t (N_f \nu) = & (-1 + \eta_\phi + \eta_V) (N_f \nu) \\ & + \frac{2}{3\pi^2} \ell_2^{(\text{F})}(0; \eta_\chi) (N_f h_V^2) h_\phi^2, \end{aligned} \quad (88)$$

$$\begin{aligned} \partial_t h_\phi^2 = & (-1 + \eta_\phi + 2\eta_\chi) h_\phi^2 \\ & - \frac{4}{\pi^2} \left( \frac{m_\phi^2}{N_f^2} \right) \ell_{1,2}^{(\text{FB})} (0, m_V^2; \eta_\chi, \eta_V) (N_f h_V^2)^2, \end{aligned} \quad (89)$$

$$\partial_t (N_f h_V^2) = (-1 + \eta_V + 2\eta_\chi) (N_f h_V^2), \quad (90)$$

$$\eta_\phi = \frac{2}{3\pi^2} m_4^{(\text{F})}(0; \eta_\chi) h_\phi^2, \quad (91)$$

$$\eta_V = \frac{4}{3\pi^2} m_4^{(\text{F})}(0; \eta_\chi) (N_f h_V^2), \quad (92)$$

$$\eta_\chi = 0, \quad (93)$$

where we have multiplied the flow equations with suitable factors of  $N_f$  in order to simplify the large- $N_f$  counting of orders. Hence, in this limit the fermion wave function renormalization does not flow,  $\eta_\chi = -\partial_t \ln Z_{\chi,k} \equiv 0$ , whereas the flow of the bosonic wave function renormalizations is nonzero.

Let us search for fixed points: assuming a fixed-point value  $m_\phi^{*2} \neq 0$ , we are forced to conclude from Eq. (83) that the scalar anomalous dimension at the fixed point obeys  $\eta_\phi^* = 2$ . Similarly, Eq. (90) requires for an interacting fixed point with  $h_V^{*2} \neq 0$  for the vector anomalous dimension  $\eta_V^* = 1$ . In fact, this is the large- $N_f$  result found in [20]. With these values of the anomalous dimensions, the full set of fixed-point values can be computed analytically, see Table II.

At this point, it may be worthwhile to make a few comments. For taking the limit  $N_f \rightarrow \infty$ , we have implicitly assumed a specific  $N_f$ -scaling of the couplings, defining the corresponding 't Hooft couplings. Since all rescaled couplings acquire finite (in particular nonzero)

TABLE II. Left columns: nonuniversal fixed-point couplings for the linear regulator and various flavor numbers  $N_f$ . Right columns: universal correlation length exponent  $\nu$ , subleading exponent  $\omega$ , and anomalous dimension  $\eta_\phi^*$ . Rough error estimates arise from the comparison to sharp cutoff results. For  $N_f \gtrsim 6$  we do not expect chiral symmetry breaking due to vector channel domination, such that the critical exponents of the Thirring fixed point do not have the same physical meaning for the long-range physics. This is indicated by the gray font of the corresponding critical exponents; see Sec. IX. For  $N_f = 2$ , a meaningful estimate of the systematic error for  $\nu$  is not available due to sharp-cutoff artifacts, see text.

$N_f$	$m_\phi^2/N_f^2$	$N_f\lambda_1$	$\lambda_2$	$h_\phi^{*2}$	$N_f h_V^{*2}/m_V^{*2}$	$\nu$	$\omega$	$\eta_\phi^*$
2	0.132	5.85	24.68	15.96	1.99	2.4(?)	1.0(2)	1.4(7)
3	0.265	16.94	39.84	19.36	6.11	1.22(2)	1.5(2)	1.6(3)
4	0.271	20.95	44.45	20.61	8.83	1.084(5)	1.7(1)	1.7(2)
5	0.266	22.70	46.55	21.41	10.83	1.043(8)	1.74(7)	1.8(1)
6	0.259	23.56	47.70	21.95	12.35	1.026(6)	1.80(4)	1.85(8)
8	0.247	24.34	48.86	22.59	14.44	1.012(3)	1.84(2)	1.91(5)
10	0.238	24.68	49.42	22.93	15.79	1.007(2)	1.79(4)	1.94(3)
12	0.231	24.85	49.73	23.14	16.74	1.004(9)	1.72(4)	1.95(2)
25	0.209	25.16	50.33	23.54	19.39	1.0006(1)	1.423(1)	1.988(2)
100	0.187	25.26	50.52	23.68	21.45	1.0000(1)	1.126(1)	1.999(1)
$\infty$	$\frac{8}{45}$ $\simeq 0.178$	$\frac{64\pi^2}{25}$ $\simeq 25.27$	$\frac{128\pi^2}{25}$ $\simeq 50.53$	$\frac{12\pi^2}{5}$ $\simeq 23.69$	$\frac{9\pi^2}{4}$ $\simeq 22.21$	1	1	2

fixed-point values, the corresponding rescalings are self-consistent and the large- $N_f$  limit is well-defined. For the original four-fermi couplings  $g_\phi = N_f h_\phi^2/m_\phi^2$  and  $g_V = N_f h_V^2/m_V^2$  this implies the large- $N_f$  scaling  $g_\phi = \mathcal{O}(1/N_f)$  and  $g_V = \mathcal{O}(1)$ , already known from the fermionic flow [49]. In fact, the fixed-point positions of  $g_\phi$  and  $g_V$  for the dynamically bosonized flow in the large- $N_f$  limit and fermionic flow exactly coincide, provided the same regulator is employed. We note, however, that the equivalence in general does not hold for the flow beyond the fixed-point regime, since kinetic terms of the bosonic fields are generated during the flow according to their finite anomalous dimensions. For instance, the large anomalous dimension  $\eta_\phi^* = 2$  indicates a rapid flow of the scalar kinetic term.

Consider the second contribution to the beta function of the scalar-fermion coupling  $h_\phi^2$  in Eq. (89), being proportional to  $m_\phi^2$ . This is exactly the contribution from the diagrams in Fig. 5, i.e., the large- $N_f$  reminiscence of the scale-dependent Hubbard-Stratonovich transformation. Without this contribution, the large- $N_f$  fixed-point equations cannot be solved with finite couplings. In other words, dynamical bosonization is crucial to find the correct large- $N_f$  behavior in the scalar sector in the present model. We have already seen an indication for this in Sec. VI, where the scalar sector completely decoupled for  $N_f \geq 4$  using only standard partial bosonization.

For the given set of integer anomalous dimensions, the large- $N_f$  fixed-point values for the vector-vector coupling  $\mu$  and the vector-scalar coupling  $\nu$  are in fact negative. We attribute this to the fact that we neglected the momentum-dependent contribution  $\propto \bar{\zeta}_k$  in Eq. (37) as well as higher order terms in the effective potential. In any case, in the large- $N_f$  limit  $\mu$  and  $\nu$  do not feed back into the flow of the remaining couplings. For consistency, we again evaluate in what follows the flow equations for

a pointlike current-current interaction,  $Z_{V,k} \rightarrow 0$ , and neglect the vector-vector selfinteractions  $\mu$  and vector-scalar interactions  $\nu$ , analogous to Sec. VI. This is expected to be a reasonable approximation as long as the vector mass  $m_V^2$  does not become too small.

## B. Fixed-point structure at general $N_f$

Beyond the large- $N_f$  limit, we evaluate the fixed-point equations numerically, both for linear and sharp cutoff. Again, we recover the known UV structure: there is one interacting Thirring fixed point for all  $1 < N_f \leq \infty$ , having only one IR relevant direction. [Recall that the case  $N_f = 1$  has been explicitly excluded in the derivation of our bosonic flow equations, cf. Eq. (44).] For small  $N_f$  the Thirring fixed point is located close to the pure scalar channel subspace, whereas for  $N_f \rightarrow \infty$  the scalar-fermion coupling becomes negligible. As we have also observed in the partially bosonized formulation in Sec. VI, the fixed-point position in this limit again exactly coincides with the fermionic fixed point. For small  $N_f$ , we find deviations from the fermionic UV structure. As the dynamically bosonized flow and the fermionic one have an identical fixed-point structure in the point-like limit (by construction), these deviations are fully related to the momentum dependence in the bosonized scalar channel. The latter is particularly important once the scalar coupling becomes long range, i.e., for small  $\bar{m}_\phi^2$ . In other words, the bosons dynamically become fluctuating relevant degrees of freedom. We depict the fixed-point positions for the linear regulator in Fig. 6, together with the corresponding values for the fermionic flow compiled from [49] for comparison. Explicit values are given in Table II. If the fixed point corresponds to a second-order phase transition as we expect it for small

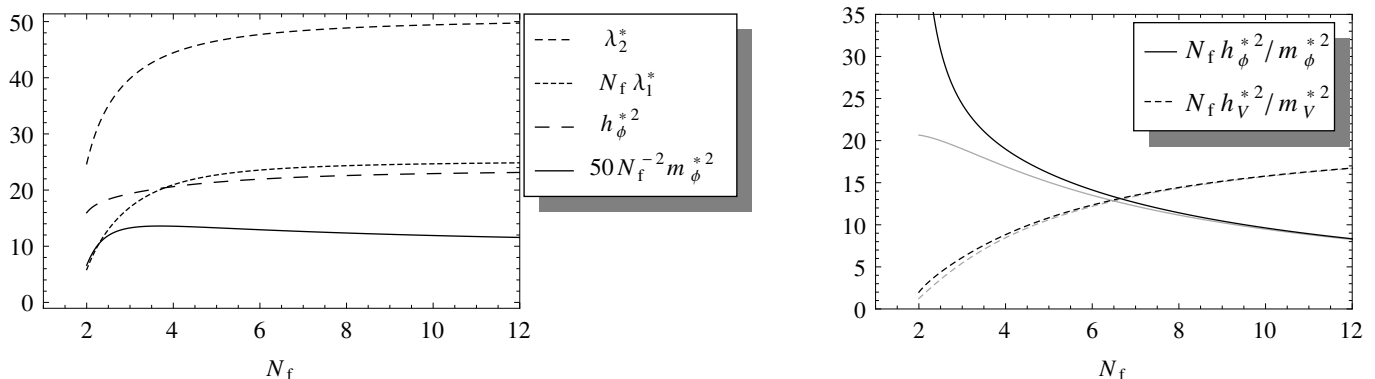


FIG. 6. Left panel: nonuniversal UV fixed-point values of dynamically bosonized RG flow for the linear regulator. The couplings have been multiplied with suitable  $N_f$  factors; for better visibility, the scalar mass has been multiplied with an additional factor 50. Right panel: Comparison of dynamically bosonized RG (black) with fermionic RG (gray). The improvement due to *dynamical* bosonization becomes obvious by comparing this plot with the left panel of Fig. 4.

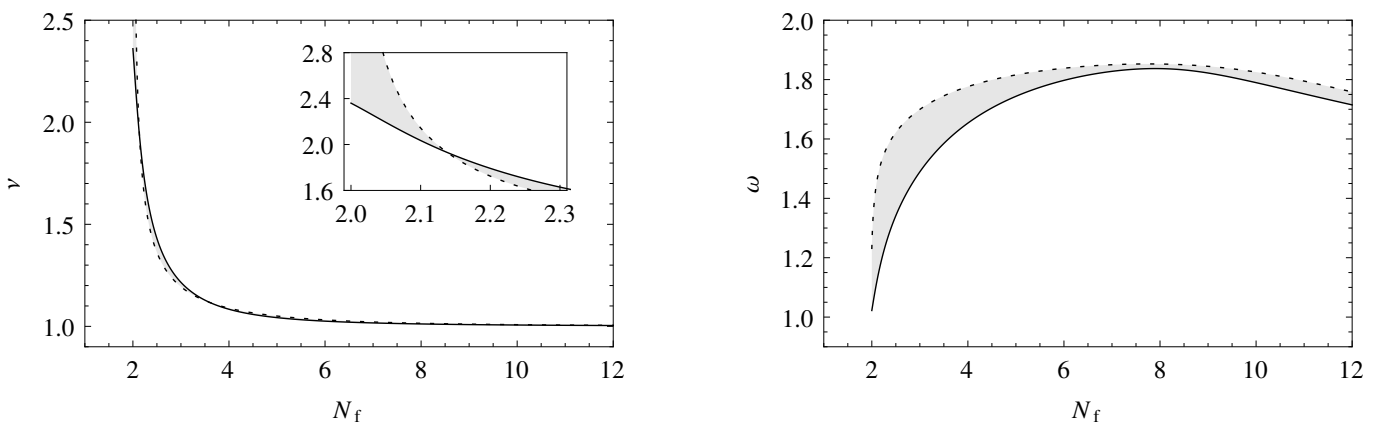


FIG. 7. Left panel: correlation length exponent  $\nu$  extracted from the linearized flow in the fixed-point regime with linear (solid) and sharp regulator (dashed). The difference (gray shaded band) serves as rough error estimate. The critical exponent is to a large extent independent of the regulator, while the uncertainty increases for  $N_f \searrow 2$ , as shown in the inset. For increasing  $N_f$  it approaches rapidly the fermionic result  $1/\Theta_1 = 1$ . Right panel: corrections-to-scaling exponent  $\omega$ .

$N_f$ , the critical behavior is uniquely determined by the fixed-point regime, where the flow can be linearized. Let  $g = (m_\phi^2, \lambda_1, \lambda_2, h_\phi^2, N_f h_V^2 / m_V^2)$  denote the vector of our (generalized) couplings. The scaling of the correlation length in the vicinity of the critical point is

$$\xi = \bar{m}_{\phi,R}^{-1} \propto |\delta g|^{-\nu} (1 + b_\pm |\delta g|^{\omega_\nu} + \dots), \quad (94)$$

with  $\delta g := g_\Lambda - g_{cr}$  measuring the distance from criticality (“reduced temperature”) and the renormalized scalar mass  $\bar{m}_{\phi,R}^2 = \lim_{k \rightarrow 0} m_\phi^2 k^2$ . By again denoting the smallest eigenvalue (being negative) of the stability matrix  $\partial \beta_i / \partial g_j|_{g^*}$  with  $-\Theta_1 < 0$  and the second smallest eigenvalue (being positive) with  $-\Theta_2 > 0$  we have for the correlation length exponent and the first subleading exponent [104]

$$\nu = 1/\Theta_1 > 0, \quad \text{and} \quad \omega = -\Theta_2 > 0. \quad (95)$$

At the critical point  $\delta g = 0$ , where the correlation length diverges, the asymptotic behavior of the scalar two-point

function is determined by the anomalous dimension  $\eta_\phi^* = \eta_\phi(g^*)$  as

$$\langle \varphi(x) \varphi(0) \rangle \propto \frac{1}{|x|^{d-2+\eta_\phi^*}}. \quad (96)$$

The critical exponents extracted from the flow in the fixed-point regime are shown in Figs. 7 and 8. We expect the values, as listed in Table II, obtained with the linear regulator to represent our most accurate results and use the difference to the sharp-cutoff results as a rough estimate on the truncation-induced error. We find that the correlation-length exponent is to a large extent regulator-independent,  $\Delta \nu / \nu \lesssim 1 \dots 2\%$  for  $N_f \gtrsim 2.1$ . Near  $N_f = 2$ , the sharp-cutoff results deviate from the linear regulator by up to a factor of two. We interpret this behavior as a large artifact of the sharp cut-off and consider the result using the linear regulator as our best estimate. For this particular case of  $N_f = 2$ , it is however difficult to estimate the systematic error. As expected, slightly larger but controlled deviations

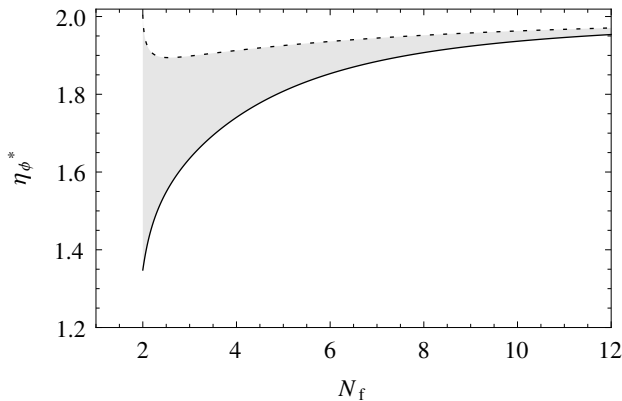


FIG. 8. Anomalous dimension  $\eta_\phi$  at the fixed point, with linear regulator (solid) and sharp regulator (dashed).

between linear and sharp cutoff occur for the anomalous dimension and the corrections-to-scaling exponent,  $\Delta\eta_\phi/\eta_\phi, \Delta\omega/\omega \lesssim 10 \dots 15\%$ . Explicit values are again given in Table II. This hierarchy of accuracy is well-known from RG studies of scalar models based on the derivative expansion [70, 80, 105].

## IX. IR BEHAVIOR AND $N_f$ -CONTROLLED QUANTUM PHASE TRANSITION

### A. Critical fermion number

If we start the flow for small  $N_f$  with initial UV couplings close to the fixed point, we find that the scalar mass eventually vanishes at some scale  $k^*$ , indicating the spontaneous breakdown of chiral symmetry. In the following, we will refer to  $k^*$  as “ $\chi$ SB scale”. Continuing the flow for  $k < k^*$  in the  $\chi$ SB regime the fermions become massive with renormalized mass  $\bar{m}_{R,f}^2 = N_f^{-1} \kappa h^2 k^2$  and the scalar sector consists of one radial mode with renormalized mass  $\bar{m}_{R,\rho}^2 = 2\kappa\lambda_1 k^2$ ,  $2N_f^2 - 1$  massive modes with  $\bar{m}_{R,\tau}^2 = N_f^{-1} \kappa\lambda_2 k^2$ , and  $2N_f^2$  massless Goldstone modes. In the deep IR  $k \rightarrow 0$ , we expect all massive modes as well as eventually the Goldstone modes to decouple, leading to IR predictions for the mass spectrum.

However, our truncation is not able to resolve this decoupling, as all couplings among the different modes are approximated by the same expansion coefficient of the effective potential. In fact, we naively find that the dimensionless parameters run into an attractive IR fixed point, such that the dimensionful masses run into a maximum and eventually decrease again for small  $k \ll k^*$ , see Fig. 9. This effect is a well-known artifact of our treatment of the effective potential, as it artificially couples the Goldstone modes to the flow of all other scalar operators. This problem can technically be solved by an adapted choice of field coordinates [106]. Here, we follow a more immediate strategy, and simply stop the flow before it enters the artificial IR fixed-point regime. For

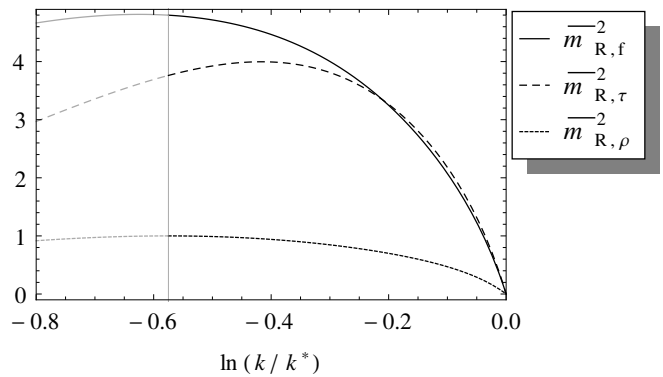


FIG. 9. RG evolution of renormalized masses in  $\chi$ SB regime for  $k < k^*$  and  $N_f = 2$ . We stop the flow when the radial mass  $\bar{m}_{R,\rho}^2$  approaches its maximum (vertical line).

our quantitative estimates, we stop the flow at the maximum of the radial mass  $\bar{m}_{R,\rho}^2$ . We have checked that the following results to a large extent do not depend on this choice. We note that the critical behavior in terms of the exponents  $\nu$  and  $\eta_\phi^*$  remains, of course, unaffected by this, since it is solely determined by the UV structure of the theory.

Once the physical scale has been set, for instance, by measuring the value of the radial mass  $\bar{m}_{R,\rho}^2$ , we can compare the dynamically generated masses among different  $N_f$ . We have already shown the renormalized fermion mass  $\bar{m}_{R,f}^2$  in units of the radial mass  $\bar{m}_{R,\rho}^2$  in Fig. 2. In Fig. 10 we now depict the renormalized scalar mass  $\bar{m}_{R,\tau}^2$  in the same units. For increasing flavor number we observe that both  $\bar{m}_{R,f}^2$  and  $\bar{m}_{R,\tau}^2$  decrease (apart from some interesting nonmonotonic behavior of the fermion mass for  $N_f \sim 3$ ) and eventually vanish for some critical flavor number  $N_f \nearrow N_f^{\text{cr}}$ . This is a clear and expected signature for a quantum phase transition governed by flavor number  $N_f$ .

Directly at  $N_f = N_f^{\text{cr}}$  we find that the vector-fermion coupling  $N_f h_V^2 / m_V^2$  diverges at the same time as the scalar mass  $m_{\phi,k}^2$  approaches zero, i.e., at the  $\chi$ SB scale  $k^*$ . We expect that this divergence is an artifact of our truncation which will be stabilized by higher terms in the vector sector [for instance, the terms  $\propto \bar{\mu}_k, \bar{\nu}_k, \bar{\zeta}_k$  in Eq. (37)]. Here, we interpret the divergence as an indication for “vector-boson-dominance” in the IR, inhibiting  $\chi$ SB. If the divergence was real, the model could exhibit dynamical Lorentz symmetry breaking [91–95]. For larger  $N_f > N_f^{\text{cr}}$  we observe the divergence already at higher scales  $k > k^*$ , inhibiting the flow to enter the  $\chi$ SB regime.

The value of  $N_f^{\text{cr}}$  can thus be obtained in two ways: First, we observe for increasing  $N_f$  a sharp decrease of the logarithm of the fermion mass once  $N_f \nearrow N_f^{\text{cr}}$ . Second, we look for the largest  $N_f$  below which the vector-fermion coupling  $N_f h_V^2 / m_V^2$  remains finite for all scales in the interval  $k \in [k^*, \Lambda]$ . Above this  $N_f$ , the vector-fermion coupling diverges before the scalar mass  $m_{\phi,k}$

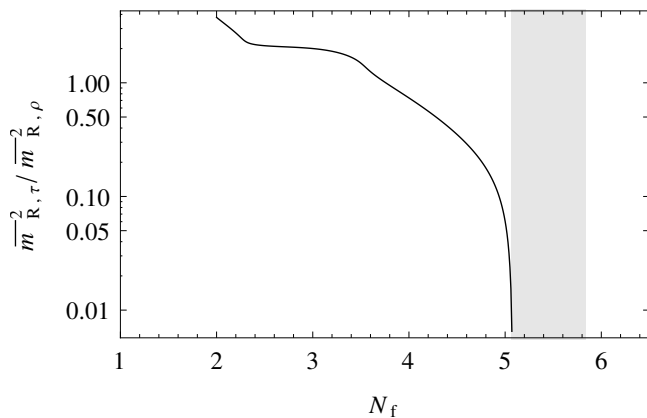


FIG. 10. Scalar mass  $\bar{m}_{R,\tau}^2$  in units of the radial mass  $\bar{m}_{R,\rho}^2$  on logarithmic scale (linear cutoff). Gray shaded area: estimates for critical flavor number  $N_f^{\text{cr}} \simeq 5.1$  (linear cutoff) and 5.8 (sharp cutoff).

approaches zero. For the linear cutoff we find  $N_f^{\text{cr}} \simeq 5.07$  with the former method and  $N_f^{\text{cr}} \simeq 5.1$  with the latter, agreeing with each other on the level of numerical precision. For the sharp cutoff, our truncation unfortunately does not allow to enter the  $\chi$ SB regime: we find  $\lambda_{1,k^*} < 0$  at the  $\chi$ SB scale, indicating the requirement of higher terms in the polynomial expansion of the effective potential (43). This is in line with optimization considerations [73, 86]: for a nonoptimized regulator (as is the sharp cutoff) a higher expansion order is needed to achieve similar predictive power. For the scalar and fermion sectors, the linear regulator by contrast satisfies standard optimization criteria [73, 86]. Nonetheless, also in the sharp-cutoff scheme, we can determine the flavor number above which the vector-fermion coupling diverges before  $m_{\phi,k} \rightarrow 0$ . From this criterion, we find  $N_f^{\text{cr}} \simeq 5.8$ . Identifying the cutoff dependence with a rough error estimate yields our result for the critical flavor number

$$N_f^{\text{cr}} \simeq 5.1(7). \quad (97)$$

This prediction represents one of the central results of this work.

### B. Thirring universality class

In the fermionic RG [49], we have shown that the “pure” Thirring model, defined by a microscopic action including only current-current interaction, is in the universality class defined by the interacting Thirring fixed point with one IR relevant coupling. Of course, this statement ultimately only holds for our specific regularization scheme, since fixed-point positions itself are nonuniversal. In the bosonized formulation developed here we can further explore the universality class of the “pure” Thirring

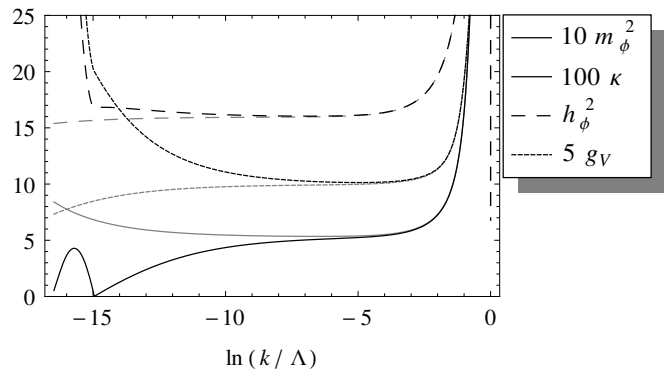


FIG. 11. RG evolution of dimensionless couplings for the “pure” Thirring model with  $N_f = 2$  and initial couplings  $m_{\phi,\Lambda}^2 = 10^6$ ,  $\lambda_{i,\Lambda} = 0$ ,  $h_{\phi,\Lambda}^2 = 0$ , and two different  $g_{V,\Lambda} = N_f h_{V,\Lambda}^2 / m_{V,\Lambda}^2$  just above (black) and below (gray)  $g_{\text{cr}}$ . Near  $\ln(k/\Lambda) \simeq -5$  the flow approaches the UV fixed-point regime. The black solid line corresponds to  $m_\phi^2$  above and  $\kappa$  below the  $\chi$ SB scale  $\ln(k^*/\Lambda) \simeq -15$ , respectively.

model by starting the flow with initial couplings

$$Z_\phi^{-1} \propto m_{\phi,\Lambda}^2 \gg 1, \quad \lambda_{i,\Lambda} \ll 1 \quad (i = 1, 2), \quad h_{\phi,\Lambda}^2 \ll 1, \quad (98)$$

i.e., with a decoupled scalar sector. In our explicit computations we use  $Z_{\phi,\Lambda} = 10^{-6}$ ,  $m_{\phi,\Lambda} = 10^6$ ,  $\lambda_{i,\Lambda} = 0$ ,  $h_{\phi,\Lambda}^2 = 0$ . However, universality guarantees that our results are independent of the exact values for the initial couplings as long as the system is governed by the corresponding fixed point. With the functional RG flow, we can explicitly verify universality. Fig. 11 shows the RG evolution of the dimensionless couplings for  $N_f = 2$  for two different initial values of the vector-fermion coupling  $g_V = N_f h_V^2 / m_V^2$  just above and below the critical value  $g_{\text{cr}}$ . Though we start with a decoupled scalar sector, the scalar couplings are rapidly generated by the RG flow, as already known from the purely fermionic RG. For initial couplings close to criticality, the flow runs from the pure Thirring axis into the fixed-point regime, which is exactly given by the Thirring fixed-point couplings in Table II, cf. Fig. 11. Thus, the critical behavior of a conventionally defined “pure” Thirring model without scalar channel in the bare action is indeed given by the universality class of our Thirring fixed point. For completeness, we show in Fig. 12 the critical coupling  $g_{\text{cr}}$  for which the flow approaches the Thirring fixed point as a function of  $N_f$ , to be compared with previous results in Ref. [49].<sup>3</sup> As in the fermionic calculation, we do not find a sharp decrease of  $1/g_{\text{cr}}$  as  $N_f \nearrow N_f^{\text{cr}}$ . This observation is in agreement with lattice simulations [27–31] but disagrees

<sup>3</sup> We use the opportunity to point out that the values for  $1/g_{\text{cr}}$  plotted in [49] include an erroneous factor of 2. This has already been corrected in [50].

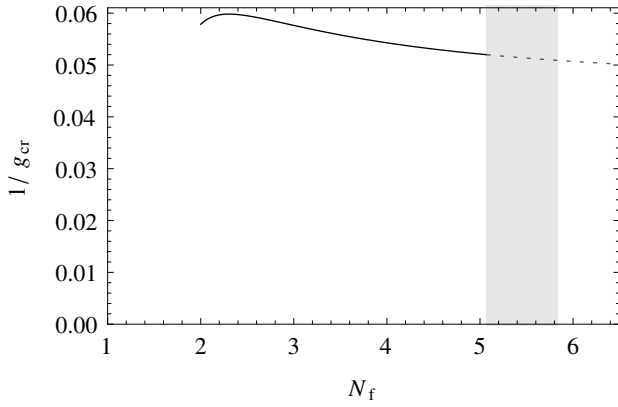


FIG. 12. Critical coupling  $1/g_{\text{cr}}$  for the “pure” Thirring model with initially decoupled scalar sector as a function of  $N_f$ . For  $N_f \gtrsim 5.1$  (gray area) we find no signature of chiral symmetry breaking (dashed line).

with earlier analytical estimates [24, 25]. A rapid variation of  $1/g_{\text{cr}}$  would have been expected if the many-flavor quantum phase transition was induced by a change in the UV fixed-point structure. This, however, is not the case in the Thirring model where the transition is rather due to a competition between the vector and scalar channel. Since the Thirring fixed point is present for all  $N_f$ , we can still determine a “would-be” critical coupling  $g_{\text{cr}}$  even for  $N_f > N_f^{\text{cr}}$  (dashed line in Fig. 12).

In order to establish the connection between the negative eigenvalues of the stability matrix  $\Theta_i$  and the critical exponents in Eq. (95) we have assumed that the propagator has a scaling form, from which one infers the hyperscaling relations [104]

$$\beta = \frac{\nu}{2}(d - 2 + \eta_\phi^*), \quad \gamma = \nu(2 - \eta_\phi^*). \quad (99)$$

The hyperscaling assumption can in fact explicitly be checked by computing directly the critical behavior of the order parameter  $\langle \varphi \rangle \propto |\delta g|^\beta$ , inverse susceptibility (unrenormalized mass)  $\chi^{-1} = \bar{m}_\rho^2 \propto |\delta g|^\gamma$ , and inverse correlation length (renormalized mass)  $\xi^{-1} = \bar{m}_{\text{R},\rho} \propto |\delta g|^\nu$ . As a function of the distance to criticality, we indeed find that the expected linear behavior on a double-log plot is excellently fulfilled; see Fig. 13 for the case of the “pure” Thirring model (initially decoupled scalar sector) and  $N_f = 2$ . The slopes of the regression lines for initial couplings on the pure Thirring axis are (for  $N_f = 2$ )

$$\beta = 2.769, \quad \gamma = 1.553, \quad \nu = 2.364, \quad (100)$$

whereas if we start the flow directly near the Thirring fixed point, we obtain

$$\beta = 2.771, \quad \gamma = 1.539, \quad \nu = 2.361. \quad (101)$$

The values should be compared with the critical exponents obtained from the linearized flow in the Thirring

fixed-point regime (see Table II), together with the hyperscaling assumption:

$$\frac{\nu}{2}(d - 2 + \eta_\phi^*) = 2.771, \quad \nu(2 - \eta_\phi^*) = 1.539, \quad \nu = 2.360, \quad (102)$$

in excellent agreement with Eqs. (101). However, hyperscaling is to a large extent also fulfilled for the conventionally defined “pure” Thirring model, cf. Eqs. (100) with (102). We attribute the small (but significant) hyperscaling violations to the presence of other fixed points: in particular the critical behavior could be influenced by fixed point  $\mathcal{B}$ , which (at least in the pointlike limit, see Fig. 1) is located in the broader vicinity of the pure Thirring axis and potentially describes a different universality class. We will further elaborate on this aspect in the following section, see also Fig. 14.

## X. COMPARISON WITH PREVIOUS STUDIES

The diversity of results for the 3d Thirring model obtained so far in the literature calls for a careful comparison of our findings with those derived with other techniques. With hindsight, this variety of partly contradictory results arises from the somewhat unexpected complexity of the model. We have identified several sources for this complexity: (i) an involved UV fixed point structure (three instead of just one UV fixed point with the Thirring fixed point being off the pure Thirring axis), (ii) a complex bound state spectrum giving rise to effective vector and scalar degrees of freedom, (iii) a symmetry breaking mechanism with competing vector and scalar channels. All issues need to be taken care of in order to arrive at conclusive answers.

Let us start with a comparison with the large- $N_f$  expansion. With standard large- $N_f$  techniques, renormalizability of the “pure” 3d Thirring model with only current-current interaction  $\propto g_V(\bar{\psi}\gamma_\mu\psi)^2$  (i.e., without scalar channel) has been shown to hold if and only if a regularization scheme is employed in which the vector field propagator remains purely transverse on the quantum level, defining an interacting UV fixed point [19–22, 107]. In Ref. [20] it is found to leading order in  $1/N_f$  (in terms of our notation)

$$\partial_t g_V = g_V \left( 1 - \frac{g_V}{g_V^*} \right), \quad \eta_V = \frac{g_V}{g_V^*}, \quad \eta_\chi = \mathcal{O}(1/N_f), \quad (103)$$

which is exactly the large- $N_f$  behavior of our flow equations (83)–(93): if the fixed point corresponds to a second-order phase transition, the corresponding correlation-length exponent is  $\nu = 1/\Theta = 1$  where  $\Theta = -\partial\beta/\partial g_V|_{g_V^*}$  and the vector field anomalous dimension is  $\eta_V(g_V^*) = 1$ .

The seeming resemblance to gauge theories has been taken even more seriously: Yang [107] claims that the

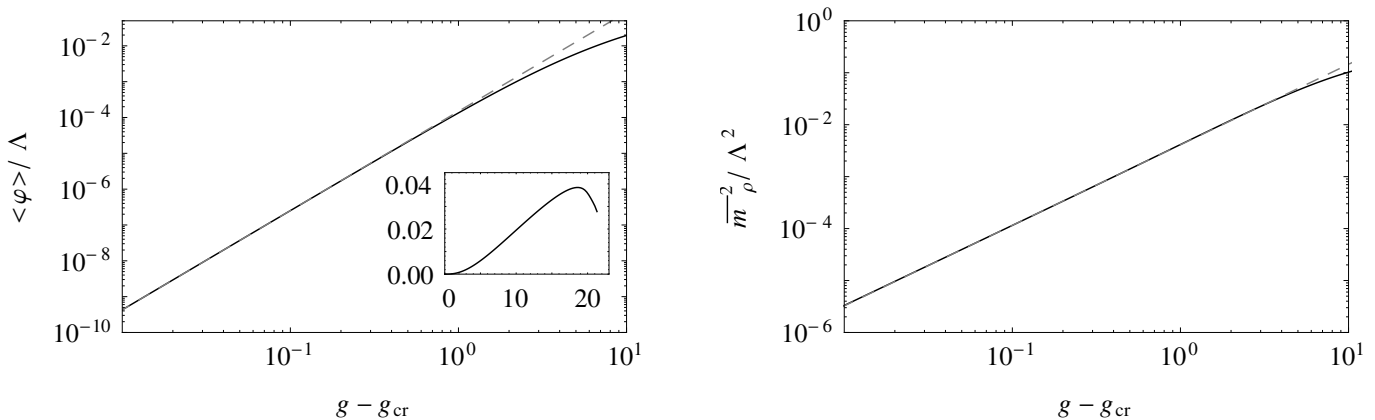


FIG. 13. Critical behavior of “pure” Thirring model with  $N_f = 2$ : order parameter  $\langle \varphi \rangle \propto |\delta g|^\beta$  (left panel) and inverse susceptibility  $\chi^{-1} = \bar{m}_\rho^2 \propto |\delta g|^\gamma$  (right panel) in double-log plot, showing the expected power law. The slope of the regression line (gray dashed) is  $\beta = 2.769$  and  $\gamma = 1.553$ , respectively. Left inset: for very large coupling on the pure Thirring axis the order parameter decreases again, see Sec. X.

partially bosonized Thirring model is equivalent to (a gauge-fixed version of) a  $U(1)$  gauge theory, in which the mass of the vector boson is generated by the Higgs mechanism. Insisting on the gauge symmetry, it is there-with argued that the coupling  $g_V$  *cannot* be renormalized. Consequently, the beta function would be vanishing for any value of  $g_V$  [21, 28].

From our functional RG viewpoint, nonperturbative renormalizability does neither rely on a specific regularization scheme nor a resemblance or equivalence to a gauge theory. All that is needed is a non-Gaussian UV fixed point (or a line of fixed points) with suitable properties to render the system asymptotically safe [51, 52]. We observe such a fixed point both in the purely fermionic description which does not have a gauge symmetry as well as in the bosonized language where the vector mass term breaks gauge symmetry manifestly. Still, it is interesting to see that our large- $N_f$  flow equations (83)–(93), resemble that of a gauge-fixed theory: the vector mass does not feed back into the vector sector and the second kinetic term ( $\sim \bar{A}_{V,k}$ ) looks like a gauge-fixing term that is even locked to the kinetic term in our truncation.

Whether or not the RG flow is eventually attracted by a gauge-invariant theory in the long-range limit still remains an open question. In our approach, this could be investigated by measuring the flow with respect to the hyperplane of actions in theory space that satisfy the (regulator-modified) Ward-Takahashi identity [73, 74, 108]. We believe, however, that this question is unrelated to that of chiral symmetry breaking, as the latter occurs in the chiral scalar sector which does not participate in the local symmetry.

The formulation of the Thirring model as a gauge theory is also at the basis of the analytical studies [22–25], which attempt to solve the Dyson-Schwinger equations (DSE) by setting the full vector propagator to its large- $N_f$  form, and the full vertex to the bare vertex (known as ladder approximation). All such studies observe the

existence of a nontrivial solution corresponding to chiral symmetry breaking for small values of  $N_f < N_f^{\text{cr}}$ . However, their predictions for the value of  $N_f^{\text{cr}}$  and the critical behavior of fermion mass and chiral order parameter differ significantly: Ref. [22] reports  $N_f^{\text{cr}} \simeq 3.24$ . Hong and Park [23] claim that symmetry breaking should persist for any value of  $N_f$ , i.e.,  $N_f^{\text{cr}} = \infty$ . In Ref. [24] an essentially singular behavior close to  $N_f^{\text{cr}} \simeq 4.32$  is found,

$$\bar{m}_{R,f} \propto \Lambda \exp\left(-\frac{2\pi}{\sqrt{N_f^{\text{cr}}/N_f - 1}}\right), \quad \text{for } N_f < N_f^{\text{cr}}, \quad (104)$$

that is to say, a phase transition of *infinite* order. Such an essential scaling law is known from a number of gauge theories, such as quenched  $\text{QED}_4$  [42, 109, 110] and  $\text{QED}_3$  with  $N_f$  fermion flavors [6–8, 15, 18], as well as many-flavor  $\text{QCD}_4$  [42, 43, 111–113]. In this context, the scaling law is often referred to as Miransky scaling; the scenario has also been termed (pseudo-)conformal phase transition [42]. Essential scaling has also been found in two-dimensional statistical systems, such as the XY model, where the scenario is called Kosterlitz-Thouless phase transition [114–117]. As has been pointed out recently [79, 118], the general mechanism being responsible for essential scaling is the merger of two RG fixed points [100, 119, 120] and their subsequent disappearance into the complex plane, or a running of a fixed point off to zero or infinite coupling. By contrast, we find that the UV Thirring fixed point persists for any  $N_f$ , hence there is no basis for and consequently no observation of essential scaling in our work.

By constructing an effective potential for the chiral order parameter  $\langle \varphi \rangle \propto \langle \bar{\psi}\psi \rangle$ , to leading order in  $1/N_f$ , Kondo [26] reports a *second-order* phase transition,

$$\langle \varphi \rangle \propto \left(\frac{N_f^{\text{cr}}}{N_f} - 1\right)^b, \quad \text{for } N_f < N_f^{\text{cr}}, \quad (105)$$

where for  $d = 3$  he finds the critical exponent  $b = 1$  and  $N_f^{\text{cr}} = 2$ . We have been motivated by these considerations to attempt a fit to our results for order parameter and fermion mass. In Fig. 3, we depict  $\langle \varphi \rangle / \bar{m}_{R,\rho}$  versus the combination  $(N_f^{\text{cr}}/N_f) - 1$  in a double-log plot. In fact, the behavior is very well compatible with a power-law scaling corresponding to a second-order phase transition at  $N_f^{\text{cr}}$ . However, the linear fit (gray line) gives  $b \simeq 0.44$  in qualitative agreement with the Kondo scenario [26] but a quantitatively differing estimate for the exponent. We emphasize that for a quantum phase transition at  $N_f^{\text{cr}}$  occurring due to competing condensation channels, the corresponding critical exponents do not have to coincide with those determining the phase transition with the coupling as control parameter. In particular, there is no reason that  $\beta|_{N_f^{\text{cr}}}$  and  $b$  should coincide. In any case, a fit to an essential scaling behavior analogous to (104) both for order parameter and fermion mass is much less successful and is not supported by our results.

Chiral symmetry breaking in the “pure” 3d Thirring model has also been investigated on the lattice [27–32]. One extensive study [31] finds  $N_f^{\text{cr}} = 6.6(1)$ , the bare value of which we consider as still consistent with our result, see below. Moreover, the study also analyzes the critical behavior close to the phase transition, both for fixed  $N_f < N_f^{\text{cr}}$  as a function of the bare coupling  $g$  and for fixed  $g > g_{\text{cr}}$  as a function of  $N_f$ . In the latter case, the data is fitted to an equation of state of the form

$$m = A \left[ (N_f - N_f^{\text{cr}}) + CL^{-\frac{1}{n}} \right] \langle \bar{\psi}\psi \rangle^p + B \langle \bar{\psi}\psi \rangle^{p+\frac{1}{b}}, \quad (106)$$

with  $m$  being the bare fermion mass (explicit symmetry-breaking parameter),  $L$  the linear extent of the system, and  $A, B, C$  some constants. Close to criticality in the chiral ( $m \rightarrow 0$ ) and thermodynamic ( $L \rightarrow \infty$ ) limit, Eq. (106) in fact reduces to the Kondo-formula (105). It is interesting to notice that the fit reported in [31] yields  $b \simeq 0.37$ , which could be considered as roughly compatible with our result  $b \simeq 0.44$ .

However, striking discrepancies occur, when one compares the critical behavior for fixed  $N_f < N_f^{\text{cr}}$  with the bare coupling as control parameter. In particular, in the sequence of studies [28–31] it is found that the exponent  $\delta$  lies between  $\delta \approx 2.8$  ( $N_f = 2$ ) and  $\delta \approx 5.8$  ( $N_f = 6$ ), i.e., most notably,  $\delta$  *increases* with  $N_f$ . The result for  $N_f = 2$  has been confirmed in a recent work [32] based on a new algorithmic approach, where the same lattice action has been employed directly in the massless-fermion limit with manifest  $U(1) \otimes U(1)$  chiral symmetry. The resulting anomalous dimension reads  $\eta_\phi^* = 0.65(1)$ , which (under the hyperscaling assumption) is equivalent to  $\delta = (5 - \eta_\phi^*)/(1 + \eta_\phi^*) = 2.64(2)$ . By contrast, we find (cf. Table II)  $\delta \approx 1.5$  ( $N_f = 2$ ) and  $\delta \approx 1.1$  ( $N_f = 6$ ), that is to say,  $\delta$  *decreases* with  $N_f$  and the values lie well

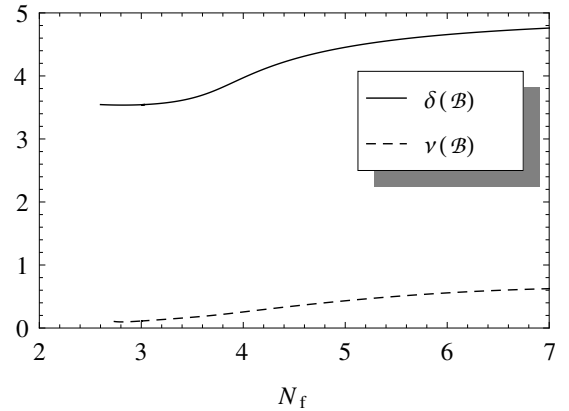


FIG. 14. Critical exponents  $\delta$  and  $\nu$  for a theory defined at the fixed point  $\mathcal{B}$  with more than one RG relevant direction; to be compared with Fig. 5 of Ref. [31].

below the above-mentioned lattice predictions<sup>4</sup>.

The lattice simulations rely on a microscopic definition of the Thirring model which is fixed by a bare action including only the Thirring-like current-current interaction. It is therefore *a priori* not clear, whether the critical behavior in the lattice models is in fact given by the Thirring fixed point, cf. the discussion in Ref. [49]. Our analysis in the preceding section VIII supports the implicit assumption that bare actions on the Thirring axis belong to the Thirring universality class for all relevant  $N_f$  (cf. Fig. 11). Nonetheless, since fixed-point positions are scheme-dependent, our results may not be directly transferable to the lattice theory. In particular, it is known from the flow in the pointlike limit, that a microscopic formulation, being fixed on the Thirring axis, could, for instance, be influenced by the fixed point  $\mathcal{B}$ , which has more than one RG relevant direction (see Fig. 1). In order to get a glimpse of how such a situation could change the corresponding critical behavior we compute in the dynamically bosonized formulation the critical exponents associated with fixed point  $\mathcal{B}$ . We emphasize however that a theory defined at  $\mathcal{B}$  in any case cannot be fixed by just one bare parameter. Naively using the hyperscaling relation<sup>5</sup>  $\delta(\mathcal{B}) = [5 - \eta_\phi^*(\mathcal{B})]/[1 + \eta_\phi^*(\mathcal{B})]$  we can relate the critical exponent  $\delta(\mathcal{B})$  to the anomalous dimension  $\eta_\phi^*(\mathcal{B})$  at  $\mathcal{B}$ , see Fig. 14. The values for  $\delta(\mathcal{B})$  lie well above those for the Thirring fixed point. Most notably,  $\delta(\mathcal{B})$  in fact now *increases* with  $N_f$ , in qualitative consistency with the behavior shown in Fig. 5 of [31]. For comparison, we also depict the correlation length exponent  $\nu = 1/\Theta_1$ , associated with the largest negative

<sup>4</sup> As a side remark we note that the DSE studies [24, 25] point to  $\delta = 2$  ( $N_f < N_f^{\text{cr}}$ ) and  $\delta = 1$  ( $N_f = N_f^{\text{cr}}$ ). (This fact has been debated in Ref. [31].) The numerical similarity to our results is probably accidental, since the nature of the transition reported in these studies substantially differs from ours; see Eq. (104) above.

<sup>5</sup> Of course, hyperscaling may not hold at a fixed point with two relevant directions.

eigenvalue of the stability matrix, i.e., the strongest RG relevant direction. In order to test this scenario lattice simulations with actions containing both invariant operators  $\sim g_V$  as well as  $g_\phi$  are needed.

However, we would like to propose yet another way to resolve this seeming contradiction between our results and lattice studies: All quoted lattice studies implement *staggered fermions*, in which case the chiral limit is more easily accessible. Exactly the same lattice action employed in the Thirring studies has also been used in simulations of the chiral  $U(1) \otimes U(1)$  Gross-Neveu ( $\chi$ GN) model in three dimensions [121], yielding  $\nu = 0.88(8)$  and  $\eta_\phi^* = 0.46(11)$ , probably consistent with the  $N_f = 2$  lattice Thirring results  $\nu = 0.85(1)$ ,  $\eta_\phi^* = 0.65(1)$  [32] and  $\nu = 0.71(4)$ ,  $\eta_\phi^* = 0.60(2)$  [28]. In fact, the symmetry breaking pattern of the lattice Thirring model in the staggered fermion formulation is [29]

$$U(N_{\text{stagg}}) \otimes U(N_{\text{stagg}}) \rightarrow U(N_{\text{stagg}}), \quad (107)$$

where  $N_{\text{stagg}}$  is the number of staggered fermion flavors. It is related to the number of continuum four-component fermions by  $N_f = 2N_{\text{stagg}}$  [122]. It is an open question whether the breaking pattern of the continuum Thirring model,

$$U(2N_f) \rightarrow U(N_f) \otimes U(N_f), \quad (108)$$

is restored in the continuum limit of the lattice Thirring model; see [28, 29] for a discussion. This scenario could be checked by a careful analysis of the low-energy spectrum in the broken phase: the number of Goldstone modes for the breaking pattern (107) would be  $N_{\text{stagg}}^2 = N_f^2/4$ , whereas for (108) one expects  $2N_f^2$  massless modes. Alternatively, one could examine the spectrum of the Dirac operator on the lattice: a necessary condition for the restoration of the full  $U(2N_f)$  symmetry in the continuum limit is that the lattice Dirac operator has to exhibit the same four-fold degeneracy of the continuum Dirac operator. In fact, for a similar strongly-coupled (2+1)-dimensional model (in the context of graphene), such a comparison reveals significant breaking of the  $U(2N_f)$  symmetry, even in the vicinity of the second-order phase transition point [123]. Unfortunately, we do not know of any such study for the Thirring model so far. If the continuum Thirring pattern (108) is not restored in the simulations, then the lattice Thirring result could possibly describe the  $\chi$ GN universality class with breaking pattern (107). In other words, the results for critical exponents would differ, simply because the continuum and the lattice models would not be in the same universality class.

We have been motivated by these consideration to compare the lattice results also to results for a fermionic  $U(N_L) \otimes U(N_R)$  model [50, 99]. For  $N_L = N_R = 1$ , a functional RG study has provided the result  $\delta_{\chi\text{GN}} = 2.58(9)$ . Interestingly enough, we observe that these  $\chi$ GN findings are in fact well consistent with the general trend reported for the lattice Thirring model, e.g.,

$\delta = 2.75(9)$  for  $N_{\text{stagg}} = 1$  [28]. [We emphasize however that  $N_{\text{stagg}} = 1$  corresponds to two four-component continuum flavors, whereas the  $U(1) \otimes U(1)$  model in Refs. [50, 99] is defined with solely one four-component fermion.] In Refs. [29, 121] the question has been raised whether for  $N_f = 2$  the distinction between  $\chi$ GN and Thirring model might be unimportant and both models might actually coincide. In such a scenario the fixed point pertaining to the  $\chi$ SB phase transition would incidentally lie in a  $U(4)$ -symmetric IR attractive subspace of the theory space. While certainly possible, we know of no argument supporting such a conjecture; it is also not favored by our results for the  $\chi$ GN and Thirring model.

In order to clarify these questions, it would be very interesting to simulate the Thirring model in a formulation in which either the restoration of the  $U(2N_f)$  symmetry can be explicitly verified in the continuum limit or in which it is manifest. In the two-component fermion formulation [Eq. (21)] the latter option might be pursued using standard methods (e.g., Wilson fermions [124]), since there is no notion of chirality in this formulation and the  $U(2N_f)$  is just a flavor symmetry. Alternatively, in the four-component language [Eq. (14)], one could employ more advanced chiral-fermion techniques, such as domain-wall [125–127] or overlap [128] fermions, both of which are explicitly chirally symmetric and deserve to be studied on their own rights due to their relevance to lattice QCD<sub>4</sub>.

We would finally like to comment on the unorthodox behavior of the chiral condensate far from the critical point, as reported in the lattice study [31]. There, it has been found that  $\langle \bar{\psi}\psi \rangle$  decreases again for large (current-current) coupling  $g_V$ . The corresponding peak position at  $g_V = g_{V,\text{max}}$  is independent of both lattice volume and bare fermion mass, indicating that its origin is at the UV scale. The effect has then been attributed to the fact that the vector propagator in the lattice regularization violates the transversity condition, the latter being crucial to the renormalizability of the  $1/N_f$  expansion. The impact of the extra divergence can however be absorbed by a coupling renormalization  $g'_V = g_V(1 - g_V/g_{V,\text{lim}})^{-1}$ , such that the strong coupling limit is recovered at  $g_V = g_{V,\text{lim}}$ .  $g_{V,\text{lim}}$  is thereupon identified with the peak position  $g_{V,\text{max}}$ .

By contrast, our RG results suggest that the 3d Thirring model can in fact be renormalized nonperturbatively without insisting on a transverse vector propagator, if one allows for a microscopic definition in the two-dimensional coupling plane spanned, for instance, by the couplings  $g_V$  and  $g_\phi$ . If this remains robust beyond our approximation, it could provide a natural explanation for the nonmonotonic behavior of the condensate as a function of  $g_V$ : Since the numerical value of any IR observable (in units of a fixed UV cutoff  $\Lambda$ ) is first and foremost given by the “duration” of RG time  $t = \ln(k/\Lambda)$  before the flow freezes out or enters the IR regime, it could well be that for a theory defined on the pure Thirring axis with bare  $g_\phi = 0$  an IR quantity decreases again

for large  $g_V$  far from criticality. Loosely speaking, just because we start the flow with a large current-current interaction does not necessarily mean that we are closer to the  $\chi$ SB regime. In order to check these considerations we have computed the order parameter for different bare couplings  $g_V$  on the Thirring axis and an initially decoupled scalar sector, showing indeed a maximum far from criticality  $g_V \gg g_{\text{cr}}$  and a subsequent decrease; see inset of Fig. 13.

## XI. CONCLUSIONS

We have studied chiral symmetry breaking in the 3d Thirring model with  $N_f$  fermion flavors. Using the functional RG equation for the effective average action, we have investigated the RG flow of the system parametrized in terms of the fundamental fermionic as well as composite bosonic degrees of freedom. We have analyzed both UV structure and IR behavior of the theory in the usual formulation with fixed fields as well as for dynamically bosonized fields, that is to say, by applying a scale-dependent Hubbard-Stratonovich transformation. Both formulations show the existence of a Thirring fixed point with one RG relevant direction. For small  $N_f$  it is located close to the scalar-channel subspace, while it approaches the vector-channel subspace (the pure Thirring axis) for increasing  $N_f$ . All this is well compatible with previous findings or indications in the purely fermionic description [49].

For entering the symmetry-broken regime, however, the description using composite bosonic fields is highly advantageous. Whereas partial bosonization has become a standard tool for functional RG analyses of strongly-correlated fermion systems, a quantitatively reliable study of the 3d Thirring model appears to require *dynamical bosonization* [67, 73, 74, 102]. The reason is that the physics of competing channels is technically affected by the Fierz ambiguity representing a challenge for many techniques based on Hubbard-Stratonovich transformations. The 3d Thirring model therefore serves as a paradigm example for the competing-channel problem and its resolution through dynamical bosonization.

For the present model, we have confirmed previous results from DSE studies and Monte-Carlo simulations indicating that chiral symmetry breaking, corresponding to a condensation in the scalar channel, occurs for large enough coupling if the number of fermion flavors  $N_f$  is smaller than a critical value  $N_f^{\text{cr}}$ , while it is shown to be absent for  $N_f > N_f^{\text{cr}}$ , independently of the coupling. We obtain the estimate  $N_f^{\text{cr}} \simeq 5.1(7)$ , where we have used regulator dependencies as an indicator for the systematic error of our approximation.

Since all previous studies we know of rely on a microscopic definition of the 3d Thirring model with pure current-current (Thirring-like) interaction, the mechanism behind the quantum phase transition at  $N_f^{\text{cr}}$  has so far been rather unclear. The present work has shown

for the first time that the critical flavor (number) may occur due to a competition between different condensation channels: the NJL-type scalar channel on the one hand, dominating for small  $N_f$  and triggering  $\chi$ SB, and the Thirring-type vector channel on the other hand, dominating for large  $N_f$  and inhibiting  $\chi$ SB. In particular, our results exclude a quantum phase transition mechanism based on fixed-point annihilation that would imply essential scaling of order parameters as a function of  $N_f^{\text{cr}} - N_f$ .

The RG approach is particularly useful for predicting the critical phenomena associated with a given universality class. We have computed the critical behavior for fixed  $N_f < N_f^{\text{cr}}$  as a function of the bare coupling in terms of the exponents  $\nu$ ,  $\eta_\phi^*$ ,  $\beta$ , and  $\gamma$  both for a microscopic definition of the model at the Thirring fixed point as well as on the pure Thirring axis (“pure” Thirring model). For  $N_f = 2$ , we have verified that the hyperscaling relations are fulfilled for UV complete models defined at the Thirring fixed point. Models with initial conditions on the pure Thirring axis necessarily inherit a certain degree of nonuniversality which becomes visible in small violations of hyperscaling, presumably induced by the vicinity of another fixed point (fixed point  $\mathcal{B}$  in our notation). Strictly speaking, the model starting on the pure Thirring axis is not itself a UV complete quantum field theory. We can, however, think of it as belonging to an RG trajectory (line of constant physics) that emanates from fixed point  $\mathcal{B}$  and thus has a definite UV completion. For the theory defined at the Thirring fixed point, we have also computed the corrections-to-scaling exponent  $\omega$ .

Close to the quantum critical point  $N_f \nearrow N_f^{\text{cr}}$ , we have discussed the scaling behavior as a function of  $N_f$  (for fixed couplings above their critical values). For the quantum phase transition as a function of  $N_f^{\text{cr}} - N_f$ , we have computed the exponent  $b \simeq 0.44$  (“magnetization exponent”), implying that there is clear evidence for the transition to be of second order. We have also computed the dynamically generated fermion mass  $\bar{m}_{\text{R},f}^2$  (fermion gap) and the  $\tau$ -mode mass  $\bar{m}_{\text{R},\tau}^2$  in units of the radial mass  $\bar{m}_{\text{R},\rho}^2$  (inverse healing length) as a function of  $N_f < N_f^{\text{cr}}$ . In principle, these are inherent predictions of our analysis and could be verified by correlator measurements in lattice simulations. Since our IR analysis is affected by an artificial non-decoupling of Goldstone modes, our quantitative estimate should, however, not be taken too literally. We consider our results on critical exponents as our most accurate quantitative predictions.

At the present stage, the long-range behavior in the vector-dominated phase for large  $N_f > N_f^{\text{cr}}$  is difficult to resolve. Our approximation with pointlike vector channel does not allow a reliable prediction of the IR properties of the system for  $N_f \gtrsim N_f^{\text{cr}}$ , since for small vector mass  $m_V^2 \lesssim \mathcal{O}(1)$  momentum-dependent terms  $\propto Z_{V,k}, \bar{A}_{V,k}, \bar{\zeta}_k$  in the effective action (37) become important as we can read off from the vector anomalous dimension growing large. In this sense, our estimate for

the critical flavor number might be a lower bound to the true value of  $N_f^{\text{cr}}$ . A larger critical flavor number could, for instance, arise from a nontrivial interplay of dynamical vector and scalar channels driving the system to criticality also for larger flavor number. Thus, we consider our findings for  $N_f^{\text{cr}}$  to be still compatible with the lattice results [31], pointing to  $N_f^{\text{cr}} \simeq 6.6$ . In any case however, it would be very interesting to see in how far the inclusion of momentum-dependent terms in the vector sector would modify the IR flow of the large- $N_f$  theory. This is in particular true for the term  $\propto \bar{\zeta}_k V_\mu V_\mu \partial_\nu V_\nu$ , which has no analogue in scalar field theories and thus could lead to a qualitatively different IR behavior as compared to the latter. Furthermore, at this point we also cannot exclude with certainty that this term does not change the UV structure of our theory in the large- $N_f$  limit. This deserves further investigation.

Whereas most [22, 24–31] (but not all [23]) of the previous studies agree at least on the very existence of a critical flavor number at order  $N_f^{\text{cr}} \sim \mathcal{O}(2\dots 7)$ , the nature of the phase transition has so far been a substantially delicate issue. Based on our detailed predictions, in particular for the transition at fixed  $N_f < N_f^{\text{cr}}$  as a function of the coupling, we believe that it may now be possible to resolve the discrepancies in the literature. For that purpose, we propose an independent investigation of the critical behavior of the 3d Thirring model, for instance, by means of a Monte Carlo simulation with a lattice action exhibiting manifest  $U(2N_f)$  symmetry.

### ACKNOWLEDGMENTS

Helpful discussions with J. Braun, S. Hands, I. Herbut, M. Huber, D. Roscher, D. Scherer, L. von Smekal, B. Wellegehausen, and A. Wipf are gratefully acknowledged. This work has been supported by the DFG under GRK 1523, FOR 723, and Gi 328/5-2.

### Appendix: Loop integrals

For self-containedness, we give here the explicit results for the loop integrals for linear and sharp cutoff. The

regulator functions  $R_k$  present in the Wetterich equation (23) may be written in terms of dimensionless shape functions  $r_k$  via

$$R_{\phi,k}(q) = Z_{\phi,k} q^2 r_{\phi,k}(q^2), \quad (\text{A.1})$$

$$R_{\psi,k}(q) = -Z_{\psi,k} q r_{\psi,k}(q^2), \quad (\text{A.2})$$

with collective bosonic and fermionic fields  $\phi = (\phi^{ab}, V_\mu, \dots)$  and  $\psi = (\psi^a, \dots)$ , respectively. The linear cutoff, which satisfies an optimization criterion [129], is defined as

$$r_{\phi,k}^{\text{opt}}(q^2) = \left( \frac{k^2}{q^2} - 1 \right) \Theta(k^2 - q^2), \quad (\text{A.3})$$

$$r_{\psi,k}^{\text{opt}}(q^2) = \left( \sqrt{\frac{k^2}{q^2}} - 1 \right) \Theta(k^2 - q^2). \quad (\text{A.4})$$

The sharp cutoff is defined as the  $a \rightarrow \infty$  limit of the class of regulators given by

$$r_{\phi,k}^{\text{sc}}(q^2) = a \left( \frac{k^2}{q^2} - 1 \right) \Theta(k^2 - q^2), \quad (\text{A.5})$$

$$r_{\psi,k}^{\text{sc}}(q^2) = \left( \sqrt{a \left( \frac{k^2}{q^2} - \frac{a-1}{a} \right)} - 1 \right) \Theta(k^2 - q^2), \quad (\text{A.6})$$

where we demand for definiteness that the sharp-cutoff limit  $a \rightarrow \infty$  is to be taken *after* the integration over the internal momentum  $q$ , i.e., after the substitution into the threshold functions [130].

The one-loop structure of the Wetterich equation guarantees that the flow equations can always be written in terms of single integrals—the threshold functions, which encode the details of the regularization scheme. Their definitions are

$$\ell_0^{(\text{B/F})d}(\omega; \eta_{\phi/\psi}) = \frac{1}{2} k^{-d} \tilde{\partial}_t \int_0^\infty dx x^{\frac{d}{2}-1} \log [P_{\phi/\psi}(x) + \omega k^2], \quad (\text{A.7})$$

$$\ell_n^{(\text{B/F})d}(\omega; \eta_{\phi/\psi}) = \frac{(-1)^n}{(n-1)!} \partial_\omega^n \ell_0^{(\text{B/F})d}(\omega; \eta_{\phi/\psi}) = -\frac{1}{2} k^{2n-d} \tilde{\partial}_t \int_0^\infty dx x^{\frac{d}{2}-1} [P_{\phi/\psi}(x) + \omega k^2]^{-n}, \quad (\text{A.8})$$

$$\ell_{n_1, n_2}^{(\text{BB})d}(\omega_1, \omega_2; \eta_\phi, \eta_V) = -\frac{1}{2} k^{2(n_1+n_2)-d} \tilde{\partial}_t \int_0^\infty dx x^{\frac{d}{2}-1} [P_\phi(x) + \omega_1 k^2]^{-n_1} [P_V(x) + \omega_2 k^2]^{-n_2}, \quad (\text{A.9})$$

$$\ell_{n_1, n_2}^{(\text{FB})d}(\omega_1, \omega_2; \eta_\psi, \eta_\phi) = -\frac{1}{2} k^{2(n_1+n_2)-d} \tilde{\partial}_t \int_0^\infty dx x^{\frac{d}{2}-1} [P_\psi(x) + \omega_1 k^2]^{-n_1} [P_\phi(x) + \omega_2 k^2]^{-n_2}, \quad (\text{A.10})$$

$$\ell_{n_1, n_2, n_3}^{(\text{FBB})d}(\omega_1, \omega_2, \omega_3; \eta_\psi, \eta_\phi) = -\frac{1}{2}k^{2(n_1+n_2+n_3)-d}\tilde{\partial}_t \int_0^\infty dx x^{\frac{d}{2}-1} [P_\psi(x) + \omega_1 k^2]^{-n_1} [P_\phi(x) + \omega_2 k^2]^{-n_2} \times [P_\phi(x) + \omega_3 k^2]^{-n_3}, \quad (\text{A.11})$$

$$m_{2,2}^{(\text{B})d}(\omega_1, \omega_2; \eta_\phi) = -\frac{1}{2}k^{6-d}\tilde{\partial}_t \int_0^\infty dx x^{\frac{d}{2}} \left[ \partial_x \frac{1}{P_\phi(x) + \omega_1 k^2} \right] \left[ \partial_x \frac{1}{P_\phi(x) + \omega_2 k^2} \right], \quad (\text{A.12})$$

$$m_2^{(\text{F})d}(\omega; \eta_\psi) = -\frac{1}{2}k^{6-d}\tilde{\partial}_t \int_0^\infty dx x^{\frac{d}{2}} \left[ \partial_x \frac{1}{P_\psi(x) + \omega k^2} \right]^2, \quad (\text{A.13})$$

$$m_4^{(\text{F})d}(\omega; \eta_\psi) = -\frac{1}{2}k^{4-d}\tilde{\partial}_t \int_0^\infty dx x^{\frac{d}{2}+1} \left[ \partial_x \frac{1+r_\psi(x)}{P_\psi(x) + \omega k^2} \right]^2, \quad (\text{A.14})$$

$$m_{1,2}^{(\text{FB})d}(\omega_1, \omega_2; \eta_\psi, \eta_{\phi/V}) = \frac{1}{2}k^{4-d}\tilde{\partial}_t \int_0^\infty dx x^{\frac{d}{2}} \frac{1+r_\psi(x)}{P_\psi(x) + \omega_1 k^2} \partial_x \frac{1}{P_{\phi/V}(x) + \omega_2 k^2}, \quad (\text{A.15})$$

with  $n_i \in \mathbb{N}$  and where we have suppressed the scale index  $k$  for the sake of simplicity. Moreover, we have abbreviated the (inverse) regularized propagator parts by

$$P_\phi(x) := x[1+r_\phi(x)], \quad P_\psi(x) := x[1+r_\psi(x)]^2. \quad (\text{A.16})$$

For the integrations, we have substituted  $q^2 \mapsto x$ , viz.,

$$\int \frac{d^d q}{(2\pi)^d} = 4v_d \int dq q^{d-1} = 2v_d \int dx x^{\frac{d}{2}-1} \quad (\text{A.17})$$

with  $v_d := \frac{1}{4}\text{Vol}(S^{d-1})/(2\pi)^d = [2^{d+1}\pi^{d/2}\Gamma(d/2)]^{-1}$ .  $\tilde{\partial}_t$  is defined to act only on the regulator's  $t$ -dependence,

$$\tilde{\partial}_t := \sum_{\Phi=\phi, V, \psi} \int dx' \frac{\partial_t [Z_\Phi r_\Phi(x')]}{Z_\Phi} \frac{\delta}{\delta r_\Phi(x')} \quad (\text{A.18})$$

$$= \int dx' x' \left\{ \frac{\partial_t [Z_\phi r_\phi(x')]}{Z_\phi} \frac{\delta}{\delta P_\phi(x')} + \frac{\partial_t [Z_V r_V(x')]}{Z_V} \frac{\delta}{\delta P_V(x')} + 2[1+r_\psi(x')] \frac{\partial_t [Z_\psi r_\psi(x')]}{Z_\psi} \frac{\delta}{\delta P_\psi(x')} \right\}. \quad (\text{A.19})$$

Both the linear and sharp regulators have the very convenient feature that all loop integrals can be performed explicitly. For the linear cutoff the results are

$$\ell_0^{(\text{B})d}(\omega; \eta_\phi) = \frac{2}{d} \left( 1 - \frac{\eta_\phi}{d+2} \right) \frac{1}{1+\omega}, \quad (\text{A.20})$$

$$\ell_n^{(\text{B})d}(\omega; \eta_\phi) = \frac{2}{d} \left( 1 - \frac{\eta_\phi}{d+2} \right) \frac{n}{(1+\omega)^{n+1}}, \quad (\text{A.21})$$

$$\ell_0^{(\text{F})d}(\omega; \eta_\psi) = \frac{2}{d} \left( 1 - \frac{\eta_\psi}{d+1} \right) \frac{1}{1+\omega}, \quad (\text{A.22})$$

$$\ell_n^{(\text{F})d}(\omega; \eta_\psi) = \frac{2}{d} \left( 1 - \frac{\eta_\psi}{d+1} \right) \frac{n}{(1+\omega)^{n+1}}, \quad (\text{A.23})$$

$$\ell_{n_1, n_2}^{(\text{BB})d}(\omega_1, \omega_2; \eta_\phi, \eta_V) = \frac{2}{d} \left[ \left( 1 - \frac{\eta_\phi}{d+2} \right) \frac{n_1}{1+\omega_1} + \left( 1 - \frac{\eta_V}{d+2} \right) \frac{n_2}{1+\omega_2} \right] \frac{1}{(1+\omega_1)^{n_1} (1+\omega_2)^{n_2}}, \quad (\text{A.24})$$

$$\ell_{n_1, n_2}^{(\text{FB})d}(\omega_1, \omega_2; \eta_\psi, \eta_\phi) = \frac{2}{d} \left[ \left( 1 - \frac{\eta_\psi}{d+1} \right) \frac{n_1}{1+\omega_1} + \left( 1 - \frac{\eta_\phi}{d+2} \right) \frac{n_2}{1+\omega_2} \right] \frac{1}{(1+\omega_1)^{n_1} (1+\omega_2)^{n_2}}, \quad (\text{A.25})$$

$$\ell_{n_1, n_2, n_3}^{(\text{FBB})d}(\omega_1, \omega_2, \omega_3; \eta_\psi, \eta_\phi) = \frac{2}{d} \left[ \left( 1 - \frac{\eta_\psi}{d+1} \right) \frac{n_1}{1+\omega_1} + \left( 1 - \frac{\eta_\phi}{d+2} \right) \left( \frac{n_2}{1+\omega_2} + \frac{n_3}{1+\omega_3} \right) \right] \times \frac{1}{(1+\omega_1)^{n_1} (1+\omega_2)^{n_2} (1+\omega_3)^{n_3}}, \quad (\text{A.26})$$

$$m_{2,2}^{(\text{B})d}(\omega_1, \omega_2; \eta_\phi) = \frac{1}{(1+\omega_1)^2 (1+\omega_2)^2}, \quad (\text{A.27})$$

$$m_2^{(\text{F})d}(\omega; \eta_\psi) = \frac{1}{(1+\omega)^4}, \quad (\text{A.28})$$

$$m_4^{(F)d}(\omega; \eta_\psi) = \frac{1}{(1+\omega)^4} + \frac{1-\eta_\psi}{d-2} \frac{1}{(1+\omega)^3} - \left( \frac{1-\eta_\psi}{2d-4} + \frac{1}{4} \right) \frac{1}{(1+\omega)^2}, \quad (\text{A.29})$$

$$m_{1,2}^{(FB)d}(\omega_1, \omega_2; \eta_\psi, \eta_{\phi/V}) = \left( 1 - \frac{\eta_{\phi/V}}{d+1} \right) \frac{1}{(1+\omega_1)(1+\omega_2)^2}. \quad (\text{A.30})$$

For the sharp cutoff we find

$$\ell_0^{(B/F)d}(\omega; \eta_{\phi/\psi}) = -\log(1+\omega) + \ell_0^{(B/F)d}(0; \eta_{\phi/\psi}), \quad (\text{A.31})$$

$$\ell_n^{(B/F)d}(\omega; \eta_{\phi/\psi}) = \frac{1}{(1+\omega)^n}, \quad (\text{A.32})$$

$$\ell_{n_1, n_2}^{(BB)d}(\omega_1, \omega_2; \eta_\phi, \eta_V) = \frac{1}{(1+\omega_1)^{n_1}(1+\omega_2)^{n_2}}, \quad (\text{A.33})$$

$$\ell_{n_1, n_2}^{(FB)d}(\omega_1, \omega_2; \eta_\psi, \eta_{\phi/V}) = \frac{1}{(1+\omega_1)^{n_1}(1+\omega_2)^{n_2}}, \quad (\text{A.34})$$

$$\ell_{n_1, n_2, n_3}^{(FBB)d}(\omega_1, \omega_2, \omega_3; \eta_\psi, \eta_\phi) = \frac{1}{(1+\omega_1)^{n_1}(1+\omega_2)^{n_2}(1+\omega_3)^{n_3}}, \quad (\text{A.35})$$

$$m_{2,2}^{(B)d}(\omega_1, \omega_2; \eta_\phi) = \frac{1}{(1+\omega_1)^2(1+\omega_2)^2}, \quad (\text{A.36})$$

$$m_2^{(F)d}(\omega; \eta_\psi) = \frac{1}{(1+\omega)^4}, \quad (\text{A.37})$$

$$m_4^{(F)d}(\omega; \eta_\psi) = \frac{1}{(1+\omega)^4}, \quad (\text{A.38})$$

$$m_{1,2}^{(FB)d}(\omega_1, \omega_2; \eta_\psi, \eta_\phi) = \frac{1}{(1+\omega_1)(1+\omega_2)^2}. \quad (\text{A.39})$$

- 
- [1] K. Novoselov, A. Geim, S. Morozov, D. Jiang, Y. Zhang, S. Dubonos, I. Grigorieva, and A. Firsov, *Science* **306**, 666 (2004).
- [2] R. D. Pisarski, *Phys. Rev.* **D29**, 2423 (1984).
- [3] J. M. Cornwall, *Phys. Rev.* **D22**, 1452 (1980).
- [4] S. Rao and R. Yahalom, *Phys. Rev.* **D34**, 1194 (1986).
- [5] T. W. Appelquist, M. J. Bowick, D. Karabali, and L. C. R. Wijewardhana, *Phys. Rev.* **D33**, 3704 (1986).
- [6] T. Appelquist, M. J. Bowick, D. Karabali, and L. C. R. Wijewardhana, *Phys. Rev.* **D33**, 3774 (1986).
- [7] T. Appelquist, D. Nash, and L. C. R. Wijewardhana, *Phys. Rev. Lett.* **60**, 2575 (1988).
- [8] D. Nash, *Phys. Rev. Lett.* **62**, 3024 (1989).
- [9] P. Maris, *Phys. Rev.* **D54**, 4049 (1996), arXiv:hep-ph/9606214.
- [10] K. Kubota and H. Terao, *Prog. Theor. Phys.* **105**, 809 (2001), arXiv:hep-ph/0101073.
- [11] K. Kaveh and I. F. Herbut, *Phys. Rev.* **B71**, 184519 (2005), arXiv:cond-mat/0411594.
- [12] S. J. Hands, J. B. Kogut, and C. G. Strouthos, *Nucl. Phys.* **B645**, 321 (2002), arXiv:hep-lat/0208030.
- [13] S. J. Hands, J. B. Kogut, L. Scorzato, and C. G. Strouthos, *Phys. Rev.* **B70**, 104501 (2004), arXiv:hep-lat/0404013.
- [14] V. P. Gusynin and M. Reenders, *Phys. Rev.* **D68**, 025017 (2003), arXiv:hep-ph/0304302.
- [15] C. S. Fischer, R. Alkofer, T. Dahm, and P. Maris, *Phys. Rev.* **D70**, 073007 (2004), arXiv:hep-ph/0407104.
- [16] A. Bashir, A. Raya, S. Sanchez-Madrigal, and C. D. Roberts, *Few Body Syst.* **46**, 229 (2009), arXiv:0905.1337 [hep-ph].
- [17] W. Li and G.-Z. Liu, *Phys. Rev.* **D81**, 045006 (2010), arXiv:1003.5299 [cond-mat.str-el].
- [18] V. P. Gusynin, V. A. Miransky, and A. V. Shpagin, *Phys. Rev.* **D58**, 085023 (1998), arXiv:hep-th/9802136.
- [19] G. Parisi, *Nucl. Phys.* **B100**, 368 (1975).
- [20] S. Hikami and T. Muta, *Prog. Theor. Phys.* **57**, 785 (1977).
- [21] S. Hands, *Phys. Rev.* **D51**, 5816 (1995), arXiv:hep-th/9411016.
- [22] M. Gomes, R. S. Mendes, R. F. Ribeiro, and A. J. da Silva, *Phys. Rev.* **D43**, 3516 (1991).
- [23] D. K. Hong and S. H. Park, *Phys. Rev.* **D49**, 5507 (1994), arXiv:hep-th/9307186.
- [24] T. Itoh, Y. Kim, M. Sugiura, and K. Yamawaki, *Prog. Theor. Phys.* **93**, 417 (1995), arXiv:hep-th/9411201.
- [25] M. Sugiura, *Prog. Theor. Phys.* **97**, 311 (1997), arXiv:hep-th/9611198.
- [26] K. Kondo, *Nucl. Phys.* **B450**, 251 (1995), arXiv:hep-th/9502070.
- [27] S. Kim and Y. Kim, arXiv:hep-lat/9605021.
- [28] L. Del Debbio, S. J. Hands, and J. C. Mehegan (UKQCD), *Nucl. Phys.* **B502**, 269 (1997), arXiv:hep-lat/9701016.
- [29] L. Del Debbio and S. J. Hands, *Nucl. Phys.* **B552**, 339 (1999), arXiv:hep-lat/9902014.

- [30] S. Hands and B. Lucini, Phys. Lett. **B461**, 263 (1999), arXiv:hep-lat/9906008.
- [31] S. Christofi, S. Hands, and C. Strouthos, Phys. Rev. **D75**, 101701 (2007), arXiv:hep-lat/0701016.
- [32] S. Chandrasekharan and A. Li, arXiv:1111.7204 [hep-lat].
- [33] D. Mesterhazy, J. Berges, and L. von Smekal, arXiv:1207.4054 [cond-mat.str-el].
- [34] G. W. Semenoff, Phys. Rev. Lett. **53**, 2449 (1984).
- [35] I. F. Herbut, Phys. Rev. Lett. **97**, 146401 (2006), arXiv:cond-mat/0606195.
- [36] I. F. Herbut, V. Juricic, and B. Roy, Phys. Rev. **B79**, 085116 (2009), arXiv:0811.0610 [cond-mat.str-el].
- [37] J. Drut and T. Lähde, Phys. Rev. Lett. **102**, 26802 (2009).
- [38] S. Hands and C. Strouthos, Phys. Rev. **B78**, 165423 (2008), arXiv:0806.4877 [cond-mat.str-el].
- [39] W. Armour, S. Hands, and C. Strouthos, Phys. Rev. **B81**, 125105 (2010), arXiv:0910.5646 [cond-mat.str-el].
- [40] V. P. Gusynin, S. G. Sharapov, and J. P. Carbotte, Int. J. Mod. Phys. **B21**, 4611 (2007), arXiv:0706.3016 [cond-mat.mes-hall].
- [41] A. Cortijo, F. Guinea, and M. A. H. Vozmediano, arXiv:1112.2054 [cond-mat.mes-hall].
- [42] V. A. Miransky and K. Yamawaki, Phys. Rev. **D55**, 5051 (1997), [Erratum-ibid.D56:3768,1997], arXiv:hep-th/9611142.
- [43] T. Appelquist, J. Terning, and L. C. R. Wijewardhana, Phys. Rev. Lett. **77**, 1214 (1996), arXiv:hep-ph/9602385.
- [44] T. Appelquist and F. Sannino, Phys. Rev. **D59**, 067702 (1999), arXiv:hep-ph/9806409 [hep-ph].
- [45] P. J. Redmond and J. L. Uretsky, Phys. Rev. Lett. **1**, 147 (1958).
- [46] K. Symanzik, Commun. Math. Phys. **45**, 79 (1975).
- [47] K. Gawedzki and A. Kupiainen, Phys. Rev. Lett. **55**, 363 (1985).
- [48] G. Felder and G. Gallavotti, Commun. Math. Phys. **102**, 549 (1986).
- [49] H. Gies and L. Janssen, Phys. Rev. **D82**, 085018 (2010), arXiv:1006.3747 [hep-th].
- [50] L. Janssen, *Critical phenomena in (2+1)-dimensional relativistic fermion systems*, Ph.D. thesis, University of Jena (2012).
- [51] S. Weinberg, in A. Zichichi, ed., *Understanding the fundamental constituents of matter* (Plenum Press, New York, 1978).
- [52] S. Weinberg, in S. Hawking and W. Israel, eds., *General Relativity* (Cambridge University Press, Cambridge, 1979), pp. 790–831.
- [53] M. Niedermaier and M. Reuter, Living Rev. Rel. **9**, 5 (2006).
- [54] R. Percacci, arXiv:0709.3851 [hep-th].
- [55] J. Braun, H. Gies, and D. D. Scherer, Phys. Rev. **D83**, 085012 (2011), arXiv:1011.1456 [hep-th].
- [56] M. Franz and Z. Tesanovic, Phys. Rev. Lett. **87**, 257003 (2001).
- [57] M. Franz, Z. Tesanovic, and O. Vafeck, Phys. Rev. **B66**, 054535 (2002), arXiv:cond-mat/0203333.
- [58] I. F. Herbut, Phys. Rev. Lett. **88**, 047006 (2002), arXiv:cond-mat/0110188.
- [59] I. F. Herbut, Phys. Rev. **B66**, 094504 (2002), arXiv:cond-mat/0202491.
- [60] I. F. Herbut, Phys. Rev. Lett. **94**, 237001 (2005), arXiv:cond-mat/0410557.
- [61] N. E. Mavromatos and J. Papavassiliou, Recent Res. Devel. Phys. **5**, 369 (2004), arXiv:cond-mat/0311421.
- [62] K. Osterwalder and R. Schrader, Commun. Math. Phys. **31**, 83 (1973).
- [63] C. Wetterich, Nucl. Phys. **B852**, 174 (2011), arXiv:1002.3556 [hep-th].
- [64] C. Wetterich, Z. Phys. **C48**, 693 (1990).
- [65] T. Baier, E. Bick, and C. Wetterich, Phys. Rev. **B62**, 15471 (2000), arXiv:cond-mat/0005218.
- [66] J. Jaeckel and C. Wetterich, Phys. Rev. **D68**, 025020 (2003), arXiv:hep-ph/0207094.
- [67] H. Gies and C. Wetterich, Phys. Rev. **D65**, 065001 (2002), arXiv:hep-th/0107221.
- [68] C. Husemann and M. Salmhofer, Phys. Rev. **B79**, 195125 (2009).
- [69] C. Wetterich, Phys. Lett. **B301**, 90 (1993).
- [70] J. Berges, N. Tetradis, and C. Wetterich, Phys. Rept. **363**, 223 (2002), arXiv:hep-ph/0005122.
- [71] K. Aoki, Int. J. Mod. Phys. **B14**, 1249 (2000).
- [72] J. Polonyi, Central Eur. J. Phys. **1**, 1 (2003), arXiv:hep-th/0110026.
- [73] J. M. Pawłowski, Annals Phys. **322**, 2831 (2007), arXiv:hep-th/0512261.
- [74] H. Gies, arXiv:hep-ph/0611146.
- [75] B. Delamotte, arXiv:cond-mat/0702365.
- [76] H. Sonoda, arXiv:0710.1662 [hep-th].
- [77] P. Kopietz, L. Bartosch, and F. Schütz, *Introduction to the functional renormalization group* (Springer Verlag, Berlin, 2010).
- [78] W. Metzner, M. Salmhofer, C. Honerkamp, V. Meden, and K. Schonhammer, arXiv:1105.5289 [cond-mat.str-el].
- [79] J. Braun, J. Phys. **G39**, 033001 (2012), arXiv:1108.4449 [hep-ph].
- [80] D. F. Litim and D. Zappala, Phys. Rev. **D83**, 085009 (2011), arXiv:1009.1948 [hep-th].
- [81] F. Benitez *et al.*, arXiv:1110.2665 [cond-mat.stat-mech].
- [82] L. Rosa, P. Vitale, and C. Wetterich, Phys. Rev. Lett. **86**, 958 (2001), arXiv:hep-th/0007093.
- [83] F. Hofling, C. Nowak, and C. Wetterich, Phys. Rev. **B66**, 205111 (2002), arXiv:cond-mat/0203588.
- [84] M. Salmhofer, C. Honerkamp, W. Metzner, and O. Lauscher, Prog. Theor. Phys. **112**, 943 (2004), arXiv:cond-mat/0409725 [cond-mat].
- [85] M. Ossadnik and C. Honerkamp, arXiv:0911.5047 [cond-mat.str-el].
- [86] D. F. Litim, Nucl. Phys. **B631**, 128 (2002), arXiv:hep-th/0203006.
- [87] R. D. Pisarski, Phys. Rev. **D44**, 1866 (1991).
- [88] V. P. Gusynin, V. A. Miransky, and I. A. Shovkovy, Phys. Rev. Lett. **73**, 3499 (1994), [Erratum-ibid.76:1005,1996], arXiv:hep-ph/9405262.
- [89] D. U. Jungnickel and C. Wetterich, Phys. Rev. **D53**, 5142 (1996), arXiv:hep-ph/9505267.
- [90] M. Q. Huber and J. Braun, arXiv:1102.5307 [hep-th].
- [91] Y. Hosotani, Phys. Lett. **B319**, 332 (1993), arXiv:hep-th/9308045.
- [92] Y. Hosotani, Phys. Rev. **D51**, 2022 (1995), arXiv:hep-th/9402096.
- [93] D. Wesolowski and Y. Hosotani, Phys. Lett. **B354**, 396 (1995), arXiv:hep-th/9505113.
- [94] K. Higashijima and N. Yokoi, Phys. Rev. **D64**, 025004 (2001), arXiv:hep-th/0101222.

- [95] V. R. Khalilov, *Theor. Math. Phys.* **140**, 1229 (2004), [*Teor. Mat. Fiz.* 140N3, 396-409 (2004)].
- [96] S. Hands, arXiv:hep-lat/9706018.
- [97] J. A. Gracey, *Int. J. Mod. Phys.* **A9**, 727 (1994), arXiv:hep-th/9306107.
- [98] A. N. Vasiliev, S. E. Derkachov, N. A. Kivel, and A. S. Stepanenko, *Theor. Math. Phys.* **94**, 127 (1993), [*Teor. Mat. Fiz.* 94, 179-192 (1993)].
- [99] H. Gies, L. Janssen, S. Rechenberger, and M. M. Scherer, *Phys. Rev.* **D81**, 025009 (2010), arXiv:0910.0764 [hep-th].
- [100] H. Gies and J. Jaeckel, *Eur. Phys. J.* **C46**, 433 (2006), arXiv:hep-ph/0507171.
- [101] J. Braun and H. Gies, *JHEP* **06**, 024 (2006), arXiv:hep-ph/0602226.
- [102] S. Floerchinger and C. Wetterich, *Phys. Lett.* **B680**, 371 (2009), arXiv:0905.0915 [hep-th].
- [103] S. Floerchinger, M. M. Scherer, and C. Wetterich, *Phys. Rev.* **A81**, 063619 (2010), arXiv:0912.4050 [cond-mat.quant-gas].
- [104] J. Zinn-Justin, *Quantum field theory and critical phenomena* (Oxford University Press, New York, 1996).
- [105] J. P. Blaizot, R. Mendez Galain, and N. Wschebor, *Phys. Lett.* **B632**, 571 (2006), arXiv:hep-th/0503103.
- [106] F. Lamprecht, Diploma thesis, University of Heidelberg (2007).
- [107] Z. Yang, Texas preprint UTTG-40-90 (1990).
- [108] U. Ellwanger, *Phys. Lett.* **B335**, 364 (1994), arXiv:hep-th/9402077 [hep-th].
- [109] P. I. Fomin, V. P. Gusynin, V. A. Miransky, and Y. A. Sitenko, *Riv. Nuovo Cim.* **6N5**, 1 (1983).
- [110] V. A. Miransky, *Nuovo Cim.* **A90**, 149 (1985).
- [111] M. Harada, M. Kurachi, and K. Yamawaki, *Phys. Rev.* **D68**, 076001 (2003), arXiv:hep-ph/0305018.
- [112] Y. Iwasaki, K. Kanaya, S. Kaya, S. Sakai, and T. Yoshie, *Phys. Rev.* **D69**, 014507 (2004), arXiv:hep-lat/0309159.
- [113] D. D. Dietrich and F. Sannino, *Phys. Rev.* **D75**, 085018 (2007), arXiv:hep-ph/0611341 [hep-ph].
- [114] V. L. Berezinsky, *Sov. Phys. JETP* **32**, 493 (1971).
- [115] V. L. Berezinsky, *Sov. Phys. JETP* **34**, 610 (1972).
- [116] J. M. Kosterlitz and D. J. Thouless, *J. Phys.* **C6**, 1181 (1973).
- [117] J. M. Kosterlitz, *J. Phys.* **C7**, 1046 (1974).
- [118] D. B. Kaplan, J.-W. Lee, D. T. Son, and M. A. Stephanov, *Phys. Rev.* **D80**, 125005 (2009), arXiv:0905.4752 [hep-th].
- [119] J. Braun and H. Gies, *JHEP* **05**, 060 (2010), arXiv:0912.4168 [hep-ph].
- [120] J. Braun, C. S. Fischer, and H. Gies, *Phys. Rev.* **D84**, 034045 (2011), arXiv:1012.4279 [hep-ph].
- [121] I. M. Barbour, N. Psycharis, E. Focht, W. Franzki, and J. Jersak (UKQCD), *Phys. Rev.* **D58**, 074507 (1998), arXiv:hep-lat/9804032.
- [122] C. Burden and A. N. Burkitt, *Europhys. Lett.* **3**, 545 (1987).
- [123] J. Giedt, A. Skinner, and S. Nayak, *Phys. Rev.* **B83**, 045420 (2011), arXiv:0911.4316 [cond-mat.str-el].
- [124] K. G. Wilson, in A. Zichichi, ed., *New Phenomena in Subnuclear Physics* (Plenum Press, New York, 1977).
- [125] D. B. Kaplan, *Phys. Lett.* **B288**, 342 (1992), arXiv:hep-lat/9206013.
- [126] Y. Shamir, *Nucl. Phys.* **B406**, 90 (1993), arXiv:hep-lat/9303005.
- [127] V. Furman and Y. Shamir, *Nucl. Phys.* **B439**, 54 (1995), arXiv:hep-lat/9405004.
- [128] H. Neuberger, *Phys. Lett.* **B417**, 141 (1998), arXiv:hep-lat/9707022.
- [129] D. F. Litim, *Phys. Rev.* **D64**, 105007 (2001), arXiv:hep-th/0103195.
- [130] M. Reuter and F. Saueressig, *Phys. Rev.* **D65**, 065016 (2002), arXiv:hep-th/0110054.